Contrib Mineral Petrol (1984) 85:209–223

Contributions to Mineralogy and Petrology


# Petrology of basalts from the Mohns-Knipovich Ridge; the Norwegian-Greenland Sea

**Else-Ragnhild Neumann**[1] **and Jean-Guy Schilling**[2]

[1] Mineralogisk-Geologisk Museum, Oslo, Norway
[2] Grad. School of Oceanography, Univ. of Rhode Island, Kingston, R.I., USA

**Abstract.** Major element compositions of submarine basalts, quenched glasses, and contained phenocrysts are reported for samples from 25 dredge stations along the Mohns-Knipovich Ridge between the Jan Mayen fracture zone and 77°30′N. Most of the basalts collected on the Jan Mayen platform have a subaerial appearance, are nepheline normative, rich in incompatible elements, and have REE-patterns strongly enriched in light-REE. The other basalts (with one exception) are tholeiitic pillow basalts, many of which have fresh quenched glass rims. From the Jan Mayen platform northeastwards the phenocryst assemblage changes from olivine ± plagioclase ± clinopyroxene ± magnetite to olivine + plagioclase ± chrome-spinel. This change is accompanied by a progressive decrease in the content of incompatible elements, light-REE enrichments and elevation of the ridge that are similar to those observed south of the Azores and Iceland hotspots. Pillow basalts and glasses collected along the esternmost part of the Mohns Ridge (450 to 675 km east of Jan Mayen) have low $K_2O$, $TiO_2$, and $P_2O_5$ contents, light-REE depleted patterns relative to chondrites, and $Mg/(Mg+Fe^{2+})$ ratios between 0.64 and 0.60. Pillow basalts and glasses from the Knipovich Ridge have similar $(Mg/Mg+Fe^{2+})$ ratios, but along the entire ridge have slightly higher concentrations of incompatible elements and chondritic to slightly light-REE enriched patterns. The incompatible element enrichment increases slightly northward. Plagioclase phenocrysts show normal and reverse zoning on all parts of the ridge whereas olivines are unzoned or show only weak normal zoning. Olivine-liquid equilibrium temperatures are calculated to be in the range of 1,060–1,206° C with a mean around 1,180° C.

Rocks and glasses collected on the Jan Mayen Platform are compositionally similar to Jan Mayen volcanic products, suggesting that off-ridge alkali volcanism on the Jan Mayen Platform is more widespread than so far suspected. There is also evidence to suggest that the alkali basalts from the Jan Mayen Platform are derived from deeper levels and by smaller degrees of partial melting of a mantle significantly more enriched in light-REE and other incompatible elements than are the tholeiitic basalts from the Eastern Mohns and Knipovich Ridge. The possibility of the presence of another hitherto unsuspected enriched mantle region north of 77°30′N is also briefly considered.

It remains uncertain whether geochemical gradients revealed in this study reflect: (1) the dynamics of mixing during mantle advection and magma emplacement into the crust along the Mid-Atlantic Ridge (MAR) spreading axis, (e.g. such as in the mantle plume – large-ion-lithophile element depleted asthenosphere mixing model previously proposed); or (2) a horizontal gradation of the mantle beneath the MAR axis similar to that observed in the overlying crust; or (3) a vertical gradation of the mantle in incompatible elements with their contents increasing with depth and derivations of melts from progressively greater depth towards the Jan Mayen Platform.

*Offprint requests to:* E.R. Neumann

## Introduction

During a cruise (EN 026) with R/V Endeavor of the University of Rhode Island in the summer of 1978, rocks were sampled from 25 dredge stations along the Mohns-Knipovich Ridge between the Jan Mayen fracture zone and 77°30′N (Fig. 1). The purpose of the cruise was to continue the mapping of chemical and isotopic variations of the basaltic layer 2A along the Mid-Atlantic Ridge (MAR) into its northernmost accessible part. Previous sampling in the area (R/V Trident and DSDP Hole 344) suggested that this is a chemically complex region (Schilling et al. 1983). It had been proposed that the chemical complexities might be caused by the existance of hotspots in the Jan Mayen area and on the Yermak plateau, northwest of Spitsbergen (Johnson and Monahan 1979; Feden et al. 1979). Alternatively, the light-REE enrichment of DSDP344 basalts could result from factors such as the youth of this part of the MAR, its probable oblique, asymetric and low rate of spreading ($<0.92$ cm $a^{-1}$ half rate, Talwani and Eldholm 1977), or its proximity to the Spitsbergen continental margin (Fig. 1).

The present paper describes the general major geological findings of the cruise, the nature of rocks recovered and discusses in detail the major and rare earth element chemistry of the lavas and their phenocrysts. Data on other trace elements and radiogenic isotopes will be presented separately (e.g., Waggoner et al. 1981, and subsequent publications). For completeness and uniformity of data, basalts dredged previously with R/V Trident at four locations on the Mohns Ridge are also included in this study.

## Sampling and geologic settings

Sample localities are shown in Fig. 1. The exact coordinates of these stations and depths of dredge haul recovery are

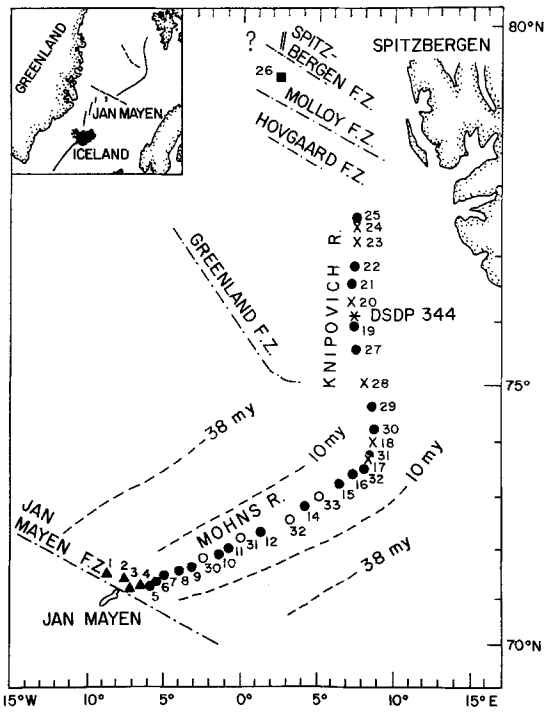


**Fig. 1.** Dredge stations of the cruises EN O26, TR 139 and DSDP344 along the Jan Mayen platform and the Mohns Knipovich Ridge. ▲ EN O26 subaerial-looking rocks; ● EN O26 basalts; × ENO26 sediments only; o TR139; * DSDP344

listed in Table 1, and descriptions of megascopic features of rocks recovered may be obtained from the authors. Dredging on the Jan Mayen Platform in the vicinity of the island (70–100 km radius) was limited to the flank of sediment-free seamounts or escarpments, since the exact location of the ridge axis remained uncertain and poorly charted in the region. The platform is structurally complex and lacks well defined magnetic anomaly lineaments. The locations of our samples in this tectonically ill-defined region are shown in Fig. 2 with respect to the bathymetric map of Perry et al. (1980).

Within the first 70 km of Jan Mayen mostly highly vesicular volcanic fragments of subaerial appearance were recovered with abundant grey mud (Stations 1D to 4D, Fig. 2). These fist-size angular fragments and well rounded cobbles were found to be generally fresh upon cutting. Although some minor glass rim and glass chips were recovered at station 1D, the first typical pillow basalts were obtained at station 5D where an elevated ridge appears to be present (Fig. 2). In order to understand the geology of the Jan Mayen Platform it is important to determine the provenance of "the subaerial-looking" basalts collected in this area.

Well developed, fresh, glassy pillow basalts and slabs were recovered on the bottom of the rift of the Mohns Ridge east of station 5D. Volcanism is clearly continuous along the Mohns Ridge axis (stations 6D to 16D, Fig. 1). Pillow basalts with gabbro and serpentinite were dredged at the station TR 139-31D with R/V Trident (Fig. 1). This

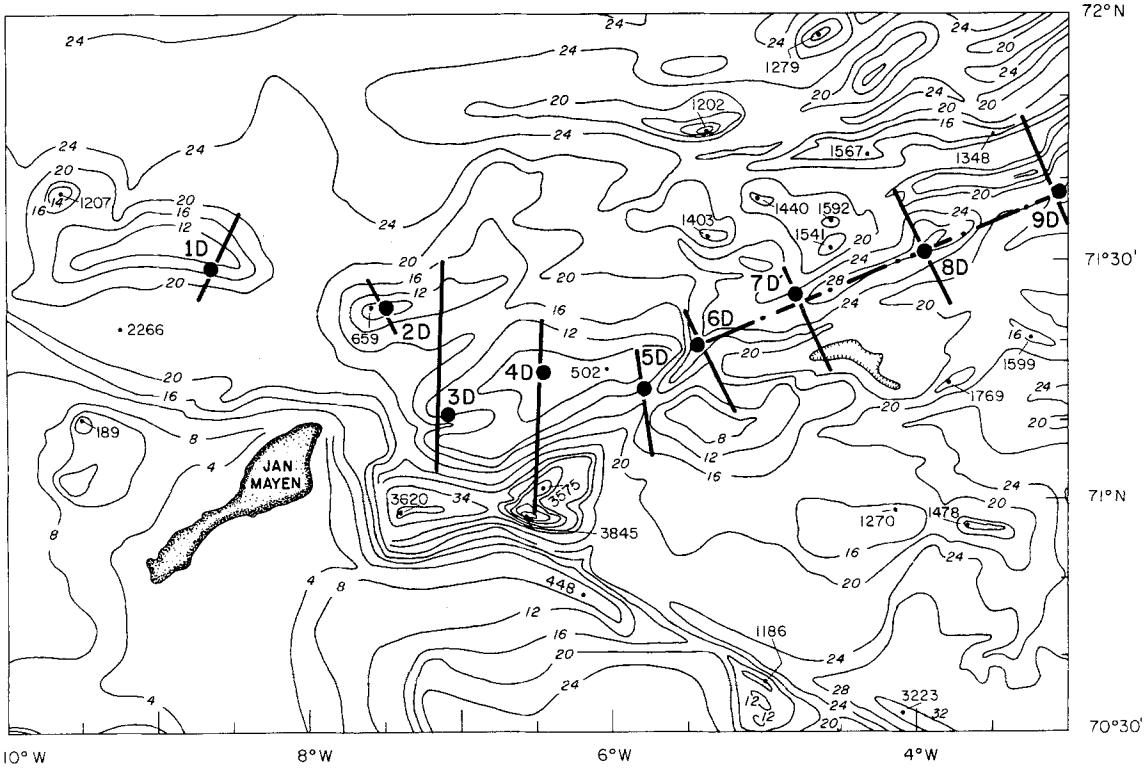


**Fig. 2.** Detailed bathymetric map of the Jan Mayen Platform (after Perry et al. 1977) with sample locations (dots) and seismic profiles (solid lines). Depth in meters. The dash-dot line shows the Mohns Ridge axis where well identified by magnetic anomalies and presence of a rift

may suggest that small fracture zone offsets are present on the Mohns Ridge despite the fact that none have been identified from magnetic lineaments (e.g. Talwani and Eldholm 1977; Vogt et al. 1981).

The Knipovich Ridge axis was found to be partly covered by sediments (Fig. 1) which include turbidite deposits. Evidence for post-sedimentation tectonic deformation and subsidence were often observed. At station 27D very fresh glassy basalts were recovered from recent eruptions which locally had clearly penetrated sediments covering the bottom of the graben. The high degree of sedimentation is attributed to the closeness of the rift to the Barents Sea shelf and the Spitsbergen continental shelf. Unsuccessful dredge hauls are also shown in Fig. 1 in order to reveal better the discontinuity of volcanism along the axis of this rather young part of the MAR. The Knipovich Ridge could not be found north of 77°40′N and seemed totally buried beneath sediments. Sampling north of the Hovgaard-Molloy FZ was impossible because of the sea ice. A dredge haul at the edge of the sea ice recovered large amounts of serpentinite criss-crossed by small veinlets of calcite, or asbestos. The station apparently was located within a yet unidentified fracture zone.

Throughout the paper, where a dredge haul station has yielded more than one type of basalt, or basalts showing different degrees of alteration, each type has been separated. A representative sample has been chosen from each group for this study; the numbers given to the individual samples from the same station are given in order of freshness or of apparent age (e.g. 4D-1, 4D-2, etc.).

For practical purposes, the description of our analytical results and discussion is done by subdividing the MAR north of Jan Mayen into four areas: (1) The Jan Mayen Platform (JMP) (0–100 km east of Jan Mayen); (2) the Western Mohns Ridge (WMR) (120–450 km east of Jan Mayen); (3) the Eastern Mohns Ridge (EMR) (450–675 km east of Jan Mayen); (4) the Knipovich Ridge (KR). We will show that this subdivision reflects important geochemical and petrological differences in the volcanic products erupted along these segments of the MAR.

## Whole rock and glass compositions

### *Major elements*

The major element compositions of the rocks and glasses are given in Table 1. The whole rock analyses were done by flame photometry (Na), atomic absorption (Mg), and X-ray fluorescence analyses of fused pellets of rock powder mixed 1:9 with sodium tetraborate (all other elements). $Fe^{2+}$ was determined by titration. Glasses and minerals were analyzed on an ARL-EMX electron microprobe equipped with a LINK energy-dispersive detector system. The rocks are listed in Table 1 according to their distance from Jan Mayen island. All Fe as $Fe^{2+}$ is termed Fe*.

*Jan Mayen Platform:* Lavas of "subaerial" appearance from the JMP (1D-2, 2D, 3D, 4D, 5D-2) are all nepheline normative and low in $SiO_2$ content (<47 wt.%). They have high $K_2O/Na_2O$ ratios (0.5–1) and relatively low Mg/(Mg+Fe*) ratios (0.43–0.58). In situ pillow basalts from the JMP are either nepheline normative (6D-1) or hypersthene-olivine normative (5D-1, 7D-1, 1D-1). Nepheline normative pillow basalts from the JMP also have low $SiO_2$ contents and $K_2O/Na_2O$ ratios greater than 0.5, in contrast to the hypersthene-olivine normative pillow basalts which have higher $SiO_2$ contents (>49%) and lower $K_2O/Na_2O$ ratios (<0.5). Stations on the JMP which contained both nepheline-normative and hyperstene-olivine normative basalts are 1D, 5D and 7D.

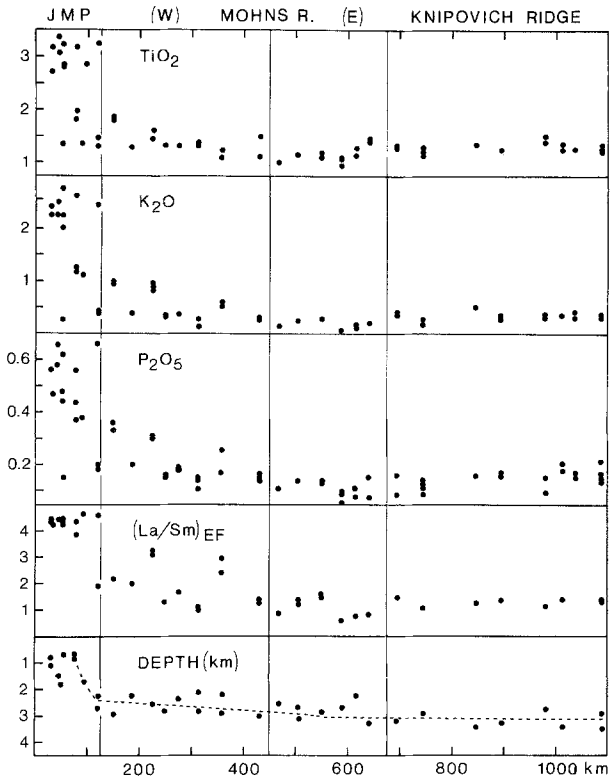


**Fig. 3.** Concentrations of $TiO_2$, $K_2O$, $P_2O_5$ in wt.%, and $(La/Sm)_{EF}$ ($(La/Sm)_{rock}/(La/Sm)_{chondrite}$) as function of sea depth and distance from Jan Mayen

*Mohns-Knipovich Ridge:* All basalts collected along the Mohns-Knipovich Ridge east of station 7D, are quartz or olivine tholeiites, with $SiO_2$ >49 wt.% and $K_2O/Na_2O$ ratios significantly less than 0.3. There is a gradual decrease in $K_2O$, $TiO_2$ and $P_2O_5$ eastward along the Mohns Ridge (Fig. 3). Rocks and glasses from the EMR have uniformly low $K_2O$, $TiO_2$ and $P_2O_5$ contents of about 0.2, 1.2 and 0.12 wt.% respectively, and Mg-values between 0.60 and 0.64. Thus, basalts from the EMR are fairly typical of normal MORB from other parts of the MAR (e.g. Schilling et al. 1983), whereas the WMR represents a transitional zone between that of normal-MORB and basalts from the JMP.

Basalts from the KR have similar Mg-values to those found on the EMR, but tend to have, uniformly along the ridge, slightly higher $Al_2O_3$, $Na_2O$, $K_2O$, $TiO_2$ and $P_2O_5$ contents and lower FeO* and MgO contents than normal MORB from the EMR.

### *Petrological provinces in the North Atlantic*

Schilling and co-workers (1983) used MAR-basalt compositions to identify two major types of petrological province in the North Atlantic, namely the Iceland Platform Province (53°–70°N) and the Azores Platform Province (28°–53°N). At any fixed Mg-value the Iceland Province is richer in Fe, Mg, and Ca than is the Azores Province, whereas the latter is richer in Si, Al, and Na. The distinction between the two provinces is most noticeable from the composition of MAR basalts erupted on the shallow platforms themselves, whereas on their periferies the differences between the two provinces tend to be more diffuse (Schilling 1973; Schilling and Sigurdsson 1979; Sigurdsson 1981; Schilling et al. 1983). The two provinces are also isotopically distinct.

**Table 1.** Sample locations, depths of recovery and major element compositions of rocks (XRF) and glasses (microprobe). EN : cruise EN 026; TR : cruise TR 139; R: rock; G: glass; *FeO: total iron as FeO

| Sample | Location | Depth | $SiO_2$ | $TiO_2$ | $Al_2O_3$ | $Fe_2O_3$ | FeO | MnO | MgO | CaO | $Na_2O$ | $K_2O$ | $P_2O_5$ | $H_2O$ | Sum |
|---|---|---|---|---|---|---|---|---|---|---|---|---|---|---|---|
| EN 3D-2 | 71°11.2′N 07°05.4′W | 1100 R | 46.27 | 2.73 | 14.85 | 2.63 | 7.97 | 0.19 | 7.26 | 11.53 | 2.30 | 2.23 | 0.47 | 0.34 | 98.77 |
| EN 2D-1 | 71°24.7′N 07°29.6′W | 890 R | 45.93 | 3.19 | 17.09 | 3.05 | 8.75 | 0.20 | 4.96 | 10.35 | 2.55 | 2.41 | 0.56 | 0.27 | 99.31 |
| EN 1D-1 | 71°29′N 08°37.6′W | 1675 R | 47.76 | 3.38 | 16.21 | 4.68 | 7.08 | 0.20 | 4.78 | 9.38 | 3.25 | 2.25 | 0.66 | 0.32 | 99.93 |
| | 71°29′N 08°37.6′W | G | 50.13 | 1.41 | 13.99 | | 12.32* | 0.19 | 7.14 | 11.99 | 2.31 | 0.11 | 0.17 | | 99.97 |
| EN 1D-2 | 71°29′N 08°37.6′W | R | 47.10 | 3.08 | 15.78 | 3.94 | 7.03 | 0.18 | 5.68 | 9.98 | 3.02 | 2.47 | 0.58 | 0.27 | 99.11 |
| EN 4D-1 | 71°15.7′N 06°29′W | 690 R | 47.57 | 2.85 | 14.46 | 2.03 | 8.68 | 0.19 | 7.04 | 10.45 | 2.92 | 2.24 | 0.48 | 0.21 | 99.12 |
| EN 4D-2 | 71°15.7′N 06°29′W | R | 46.79 | 3.22 | 16.90 | 3.59 | 6.96 | 0.18 | 4.33 | 10.19 | 2.87 | 2.76 | 0.62 | 0.63 | 99.04 |
| EN 4D-3 | 71°15.7′N 06°29′W | R | 46.93 | 2.80 | 15.03 | 2.80 | 8.16 | 0.19 | 7.13 | 11.53 | 2.44 | 2.03 | 0.44 | 0.12 | 99.60 |
| EN 5D-1 | 71°14.3′N 05°46.9′W | 750 R | 49.04 | 1.96 | 15.15 | 2.26 | 7.87 | 0.17 | 6.53 | 11.08 | 2.49 | 1.17 | 0.37 | 0.59 | 98.68 |
| EN 5D-2 | 71°14.3′N 05°46.9′W | R | 46.74 | 3.20 | 16.97 | 2.02 | 9.24 | 0.20 | 4.65 | 10.00 | 2.97 | 2.62 | 0.56 | 0.24 | 99.41 |
| EN 5D-3 | 71°14.3′N 05°46.9′W | R | 46.41 | 1.83 | 17.45 | 2.84 | 6.22 | 0.16 | 6.86 | 11.96 | 2.39 | 1.23 | 0.44 | 1.19 | 98.98 |
| EN 6D-1 | 71°19.5′N 05°25.6′W | 1725 R | 47.17 | 1.38 | 15.58 | 2.33 | 5.13 | 0.14 | 10.66 | 12.89 | 2.17 | 1.12 | 0.38 | 0.93 | 99.88 |
| EN 7D-1 | 71°26′N 04°47.6′W | 2490 R | 50.47 | 1.31 | 14.77 | 1.36 | 8.25 | 0.17 | 8.66 | 11.01 | 2.30 | 0.40 | 0.18 | 0.67 | 99.55 |
| | 71°26′N 04°47.6′W | G | 50.11 | 1.48 | 14.79 | | 9.33* | 0.17 | 7.87 | 10.91 | 2.54 | 0.46 | 0.20 | | 97.86 |
| EN 7D-2 | 71°26′N 04°47.6′W | R | 48.09 | 3.27 | 15.67 | 4.25 | 6.89 | 0.20 | 4.92 | 9.43 | 3.28 | 2.45 | 0.66 | 0.26 | 99.37 |
| EN 8D-1 | 71°31.8′N 03°56.3′W | 2925 R | 52.08 | 1.84 | 14.76 | 2.20 | 8.69 | 0.18 | 5.25 | 8.85 | 2.95 | 0.94 | 0.36 | 1.60 | 99.70 |
| | 71°31.8′N 03°56.3′W | G | 52.64 | 2.17 | 14.25 | | 12.29* | 0.07 | 3.90 | 8.16 | 2.89 | 1.04 | 0.62 | | 98.24 |
| EN 8D-2 | 71°31.8′N 03°56.3′W | R | 52.07 | 1.86 | 14.74 | 1.92 | 8.98 | 0.18 | 5.46 | 8.78 | 2.96 | 0.98 | 0.33 | 2.00 | 100.26 |
| | 71°31.8′N 03°56.3′W | G | 53.21 | 2.17 | 14.21 | | 11.83* | 0.21 | 4.06 | 8.48 | 3.20 | 0.94 | 0.45 | | 98.96 |
| EN 9D-1 | 71°38.5′N 03°03.4′W | 2220 R | 51.17 | 1.31 | 15.29 | 1.64 | 7.61 | 0.16 | 7.71 | 11.19 | 2.39 | 0.41 | 0.20 | 0.52 | 99.60 |
| | 71°38.5′N 03°03.4′W | G | 51.61 | 1.36 | 15.66 | | 9.08* | 0.17 | 7.75 | 11.46 | 2.70 | 0.36 | 0.20 | | 100.27 |
| TR 30D-1 | 71°49′N 02°04.5′W | 2460 R | 48.70 | 1.46 | 14.74 | 1.55 | 7.12 | 0.15 | 8.83 | 10.48 | 2.28 | 0.98 | 0.31 | 2.64 | 99.64 |
| TR 30D-2 | 71°49′N 02°04.5′W | R | 49.32 | 1.45 | 14.78 | 1.43 | 7.28 | 0.15 | 9.03 | 10.51 | 2.53 | 0.90 | 0.30 | 2.26 | 99.94 |
| | 71°49′N 02°04.5′W | G | 49.88 | 1.63 | 15.30 | | 8.51* | 0.21 | 7.64 | 10.96 | 2.70 | 0.82 | 0.29 | | 97.94 |
| EN 10D-1 | 71°53.3′N 01°23.6′W | 2900 R | 50.68 | 1.32 | 15.19 | 2.47 | 7.52 | 0.17 | 7.76 | 11.32 | 2.43 | 0.30 | 0.16 | 0.44 | 99.76 |
| | 71°53.3′N 01°23.6′W | G | 50.33 | 1.37 | 15.39 | | 9.08* | 0.20 | 7.60 | 11.22 | 2.63 | 0.32 | 0.00 | | 98.14 |
| EN 10D-2 | 71°53.3′N 01°23.6′W | R | 50.55 | 1.33 | 15.28 | 1.71 | 8.28 | 0.17 | 7.90 | 11.33 | 2.37 | 0.36 | 0.15 | 0.58 | 100.01 |
| EN 11D-1 | 71°59.5′N 00°39.0′W | 2340 R | 50.75 | 1.33 | 15.15 | 1.42 | 8.34 | 0.17 | 8.25 | 11.19 | 2.39 | 0.38 | 0.19 | 0.52 | 100.08 |
| | 71°59.5′N 00°39.0′W | G | 50.89 | 1.34 | 15.27 | | 9.61* | 0.06 | 7.67 | 11.20 | 2.61 | 0.38 | 0.18 | | 99.31 |
| TR 31D-1 | 72°10.5′N 00°14′E | 2460 R | 50.31 | 1.29 | 15.19 | 1.71 | 7.99 | 0.17 | 7.97 | 11.54 | 2.51 | 0.23 | 0.11 | 0.62 | 99.71 |
| | 72°10.5′N 00°14′E | G | 50.84 | 1.39 | 15.62 | | 9.33* | 0.06 | 7.91 | 11.52 | 2.69 | 0.15 | | | 99.51 |
| TR 31D-2 | 72°10.5′N 00°14′E | R | 50.40 | 1.30 | 15.32 | 1.70 | 8.06 | 0.17 | 8.14 | 11.51 | 2.44 | 0.23 | 0.15 | 0.55 | 99.97 |
| | 72°10.5′N 00°14′E | G | 50.62 | 1.37 | 15.19 | | 9.68* | 0.06 | 7.66 | 11.58 | 2.73 | 0.22 | 0.11 | | 99.22 |
| EN 12D-2 | 72°19.4′N 01°28.9′E | 2525 R | 51.15 | 1.22 | 15.60 | 1.28 | 6.98 | 0.15 | 7.68 | 11.86 | 2.53 | 0.62 | 0.26 | 0.64 | 99.97 |
| | 72°19.4′N 01°28.9′E | G | 51.09 | 1.27 | 15.78 | | 8.07* | 0.14 | 7.60 | 11.83 | 2.77 | 0.60 | 0.26 | | 99.41 |
| EN 12D-3 | 72°19.4′N 01°28.9′E | R | 50.70 | 1.09 | 16.45 | 1.33 | 6.50 | 0.14 | 8.58 | 12.12 | 2.12 | 0.53 | 0.17 | 0.64 | 100.37 |
| TR 32D-1 | 72°36.5′N 03°22.5′E | 3020 R | 50.86 | 1.15 | 15.26 | 1.67 | 7.25 | 0.16 | 9.13 | 11.67 | 2.27 | 0.32 | 0.14 | 0.53 | 100.41 |
| | 72°36.5′N 03°22.5′E | G | 50.93 | 1.15 | 15.59 | | 8.27* | 0.21 | 8.40 | 11.93 | 2.54 | 0.28 | 0.17 | | 99.54 |
| TR 32D-2 | 72°36.5′N 03°22.5′E | R | 50.52 | 1.10 | 15.03 | 1.59 | 7.41 | 0.16 | 9.36 | 11.48 | 2.22 | 0.26 | 0.14 | 0.55 | 99.82 |
| | 72°36.5′N 03°22.5′E | G | 50.50 | 1.51 | 15.80 | | 8.75* | 0.21 | 7.20 | 10.74 | 2.97 | 0.29 | 0.15 | | 98.12 |
| EN 14D-1 | 72°48.8′N 04°15.8′E | 2540 R | 50.38 | 1.01 | 17.57 | 1.18 | 6.93 | 0.14 | 7.35 | 12.34 | 2.26 | 0.13 | 0.11 | 0.28 | 99.78 |
| | 72°48.8′N 04°15.8′E | G | 50.52 | 1.17 | 15.08 | | 9.77* | 0.19 | 7.77 | 12.11 | 2.55 | 0.25 | 0.17 | | 99.74 |
| TR 33D-1 | 73°00.5′N 05°11′E | 2850 R | 50.43 | 1.13 | 14.92 | 1.56 | 7.84 | 0.16 | 9.63 | 11.21 | 2.36 | 0.23 | 0.14 | 0.47 | 100.08 |
| TR 33D-2 | 73°00.5′N 05°11′E | R | 50.60 | 1.14 | 14.90 | 1.41 | 7.89 | 0.16 | 9.72 | 11.20 | 2.28 | 0.23 | 0.14 | 0.42 | 100.09 |
| EN 15D-1 | 73°12.9′N 06°26.3′E | 2840 R | 50.58 | 1.09 | 15.19 | 1.46 | 7.56 | 0.16 | 9.25 | 11.50 | 2.19 | 0.28 | 0.13 | 0.50 | 99.89 |
| | 73°12.9′N 06°26.3′E | G | 50.09 | 1.21 | 15.33 | | 8.29* | 0.19 | 7.93 | 11.42 | 2.19 | 0.31 | 0.13 | | 97.09 |
| EN 15D-2 | 73°12.9′N 06°26.3′E | R | 50.36 | 1.09 | 15.26 | 1.47 | 7.52 | 0.17 | 8.92 | 11.50 | 2.19 | 0.27 | 0.14 | 0.61 | 99.50 |
| | 73°12.9′N 06°26.3′E | G | 49.82 | 1.22 | 15.41 | | 8.88* | 0.26 | 7.77 | 11.92 | 2.47 | 0.34 | 0.28 | | 98.52 |
| EN 16D-1 | 73°24.3′N 07°23.3′E | 2620 R | 50.84 | 1.08 | 16.24 | 1.12 | 7.60 | 0.16 | 8.45 | 12.04 | 2.33 | 0.06 | 0.10 | 0.32 | 100.34 |
| | 73°24.3′N 07°23.3′E | G | 50.83 | 0.94 | 15.76 | | 8.79* | 0.14 | 8.28 | 11.89 | 2.42 | 0.09 | 0.06 | | 99.39 |
| EN 16D-2 | 73°24.3′N 07°23.3′E | R | 50.61 | 1.10 | 15.97 | 1.32 | 7.74 | 0.16 | 8.65 | 12.08 | 2.39 | 0.07 | 0.09 | 0.25 | 100.43 |
| EN 32D-1 | 73°31.2′N 08°06.5′E | 2290 R | 50.28 | 1.14 | 16.15 | 1.23 | 7.76 | 0.16 | 8.24 | 11.77 | 2.50 | 0.13 | 0.11 | 0.22 | 99.69 |
| | 73°31.2′N 08°06.5′E | G | 50.48 | 1.21 | 15.83 | | 8.67* | 0.18 | 8.49 | 11.60 | 2.65 | 0.13 | | | 99.24 |
| EN 32D-3 | 73°31.2′N 08°06.5′E | R | 50.47 | 1.15 | 15.73 | 1.47 | 7.69 | 0.16 | 8.49 | 11.67 | 2.54 | 0.17 | 0.11 | 0.41 | 100.06 |
| | 73°31.2′N 08°06.5′E | G | 50.49 | 1.29 | 15.69 | | 9.23* | 0.13 | 8.27 | 11.85 | 2.70 | 0.16 | 0.08 | | 99.89 |
| EN 31D-1 | 73°44.6′N 08°22.3′E | 3290 R | 50.19 | 1.40 | 15.04 | 1.97 | 7.70 | 0.17 | 8.39 | 10.95 | 2.73 | 0.20 | 0.15 | 0.99 | 99.88 |
| | 73°44.6′N 08°22.3′E | G | 50.49 | 1.47 | 15.63 | | 9.29* | 0.19 | 7.82 | 11.05 | 2.90 | 0.19 | 0.08 | | 99.11 |
| EN 30D-1 | 74°11.7′N 08°50.1′E | 3210 R | 51.12 | 1.29 | 15.23 | 1.06 | 7.62 | 0.15 | 8.63 | 10.72 | 2.56 | 0.37 | 0.16 | 0.48 | 99.39 |
| | 74°11.7′N 08°50.1′E | G | 50.26 | 1.35 | 15.30 | | 8.13* | 0.23 | 7.77 | 10.66 | 2.82 | 0.40 | 0.09 | | 97.01 |
| EN 29D-1 | 74°39.2′N 08°30.7′E | 2880 R | 51.15 | 1.14 | 15.84 | 1.17 | 7.14 | 0.15 | 8.13 | 11.80 | 2.52 | 0.23 | 0.11 | 0.63 | 100.01 |
| | 74°39.2′N 08°30.7′E | G | 51.20 | 1.21 | 16.00 | | 8.05* | 0.18 | 8.25 | 11.65 | 2.74 | 0.21 | 0.09 | | 99.58 |
| EN 29D-2 | 74°39.2′N 08°30.7′E | R | 50.98 | 1.15 | 15.85 | 1.20 | 7.28 | 0.15 | 8.43 | 11.63 | 2.56 | 0.28 | 0.13 | 0.44 | 100.08 |
| | 74°39.2′N 08°30.7′E | G | 50.28 | 1.30 | 15.51 | | 7.69* | 0.13 | 7.86 | 11.65 | 2.74 | 0.20 | 0.14 | | 97.50 |
| EN 27D-2 | 75°31.4′N 07°30.2′E | 3460 R | 51.59 | 1.34 | 15.95 | 1.63 | 6.94 | 0.15 | 7.01 | 10.67 | 2.98 | 0.50 | 0.16 | 0.82 | 99.74 |
| EN 19D-1 | 75°57.8′N 07°16.9′E | 3260 R | 50.75 | 1.24 | 16.23 | 1.27 | 6.64 | 0.14 | 8.87 | 10.76 | 3.00 | 0.36 | 0.17 | 0.55 | 99.98 |
| | 75°57.8′N 07°16.9′E | G | 51.49 | 1.27 | 16.93 | | 7.46* | 0.15 | 7.72 | 10.92 | 3.14 | 0.30 | 0.16 | | 99.54 |

**Table 1** (continued)

| Sample | Location | Depth | $SiO_2$ | $TiO_2$ | $Al_2O_3$ | $Fe_2O_3$ | FeO | MnO | MgO | CaO | $Na_2O$ | $K_2O$ | $P_2O_5$ | $H_2O$ | Sum |
|---|---|---|---|---|---|---|---|---|---|---|---|---|---|---|---|
| EN 21D-1 | 76°33.4′N 07°11.3′E | 2810 R | 50.88 | 1.41 | 15.98 | 1.39 | 7.72 | 0.17 | 8.11 | 10.80 | 2.79 | 0.29 | 0.15 | 0.63 | 100.32 |
| | 76°33.4′N 07°11.3′E | G | 51.09 | 1.54 | 16.09 | | 8.76* | 0.10 | 7.50 | 10.64 | 3.36 | 0.36 | 0.10 | | 99.54 |
| EN 22D-1 | 76°51.3′N 07°22.3′E | 3450 R | 51.37 | 1.24 | 15.88 | 1.19 | 7.00 | 0.15 | 8.61 | 11.05 | 2.72 | 0.34 | 0.18 | 0.56 | 100.29 |
| | 76°51.3′N 07°22.3′E | G | 51.04 | 1.39 | 15.79 | | 8.04* | 0.09 | 7.27 | 11.30 | 3.07 | 0.38 | 0.21 | | 98.58 |
| EN 22D-2 | 76°51.3′N 07°22.3′E | R | 51.05 | 1.25 | 15.93 | 1.30 | 6.86 | 0.15 | 8.82 | 11.12 | 2.86 | 0.34 | 0.18 | 0.52 | 100.38 |
| | 76°51.3′N 07°22.3′E | G | 52.21 | 1.47 | 16.16 | | 8.59* | 0.14 | 7.25 | 11.53 | 1.58 | 0.38 | 0.42 | | 99.87 |
| EN 25D-1 | 77°31.7′N 07°40.3′E | 2920 R | 51.20 | 1.27 | 16.36 | 1.34 | 6.72 | 0.15 | 7.94 | 11.34 | 2.89 | 0.30 | 0.15 | 0.43 | 100.09 |
| | 77°31.7′N 07°40.3′E | G | 51.47 | 1.35 | 15.98 | | 8.24* | 0.16 | 7.48 | 11.22 | 3.04 | 0.29 | 0.22 | | 99.57 |
| EN 25D-2 | 77°31.7′N 07°40.3′E | R | 50.64 | 1.23 | 16.54 | 1.45 | 6.54 | 0.15 | 8.29 | 11.67 | 2.86 | 0.40 | 0.17 | 0.55 | 100.49 |
| | 77°31.7′N 07°40.3′E | G | 50.31 | 1.29 | 16.53 | | 8.01* | 0.22 | 7.95 | 11.61 | 2.92 | 0.32 | 0.14 | | 99.30 |

**Table 2.** Mean compositions (standard deviations in parantheses) of analyzed glasses with $Mg/(Mg+Fe^*) = 0.60–0.65$, compared with MAR basalts within the same $Mg/(Mg+Fe^*)$ range from the Azores Province (34°–53°N) and the Iceland Province (53°–70°N) as defined by Sigurdsson (1981) and Schilling et al. (1983)

| $\frac{Mg}{Mg+Fe^*}$ | Jan Mayen | W Mohns R | E Mohns R | Knipovich R | Azores P 34°–53° | Iceland P 53°–70° |
|---|---|---|---|---|---|---|
| | 2 samples | 9 samples | 7 samples | 9 samples | 21 samples | 7 samples |
| $SiO_2$ | 50.29 (0.25) | 50.76 (0.60) | 50.38 (0.26) | 51.04 (0.53) | 51.01 (0.97) | 49.39 (0.71) |
| $TiO_2$ | 1.41 (0.10) | 1.36 (0.16) | 1.22 (0.19) | 1.34 (0.10) | 1.43 (0.32) | 1.07 (0.15) |
| $Al_2O_3$ | 15.14 (0.49) | 15.56 (0.18) | 15.53 (0.19) | 16.02 (0.49) | 15.27 (0.68) | 15.11 (0.31) |
| FeO* | 9.02 (0.44) | 8.72 (0.51) | 8.99 (0.48) | 8.11 (0.49) | 9.38 | 10.27 |
| MnO | 0.15 (0.01) | 0.17 (0.06) | 0.18 (0.04) | 0.16 (0.05) | 0.14 (0.04) | 0.13 (0.04) |
| MgO | 7.99 (0.16) | 7.82 (0.31) | 8.05 (0.28) | 7.67 (0.10) | 7.81 (0.51) | 8.65 (0.31) |
| CaO | 11.32 (0.58) | 11.50 (0.33) | 11.69 (0.36) | 11.24 (0.41) | 11.71 (0.45) | 12.98 (1.00) |
| $Na_2O$ | 2.47 (0.11) | 2.67 (0.08) | 2.55 (0.23) | 2.82 (0.50) | 2.52 (0.49) | 2.10 (0.15) |
| $K_2O$ | 0.35 (0.16) | 0.42 (0.24) | 0.21 (0.08) | 0.32 (0.07) | 0.26 (0.25) | 0.05 (0.03) |
| $P_2O_5$ | 0.18 (0.04) | 0.18 (0.11) | 0.07 (0.05) | 0.14 (0.05) | 0.11 (0.11) | 0.03 (0.05) |

Relative to normal MORB, MAR basalts over the Azores Platform have lower ratios of $^3He/^4He$ whereas over Iceland they are higher. Schilling and co-workers have shown that, on the Kolbeinsey Ridge from 70°N up to the Jan Mayen FZ, and the few R/V Trident stations previously sampled on the Mohns Ridge, MORB tended to resemble those of the Azores Province and this appears also true in terms of $^3He/^4He$ ratios (Kurz et al. 1982; Poreda et al. 1982).

The detailed study of the Mohns-Knipovich Ridge basalts reported here further corroborate this early inference. The comparison is made in Table 2. At a fixed Mg-value, the MAR north of Jan Mayen is clearly a province rich in silica and alkalies and low in iron, magnesium and calcium relative to Iceland Province basalts, but resemble those from the Azores Province. This is illustrated for example on an AFM diagram (Fig. 4). However, Fig. 4 also shows that the MAR basalt population of the Greenland-Norwegian Sea can be further subdivided according to alkali content. At a fixed MgO/FeO ratio, tholeiites from the KR are richest in alkalies, the EMR the lowest, and the WMR intermediate. Nepheline normative basalts from the JMP follow similar trends to moderately fractionated basalt series from many oceanic islands (e.g. LeMaitre 1962).

The compositional gradient found along the WMR is

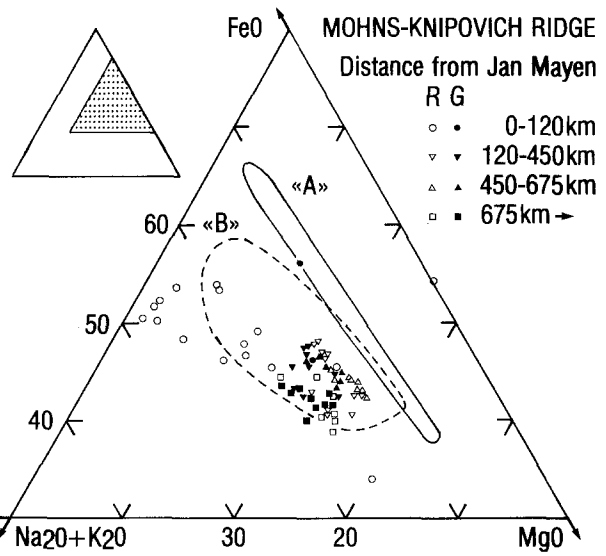


**Fig. 4.** Basalt analyses projected into the AFM-plane (wt.%), as compared to MOR basalts from other parts of the Mid-Atlantic Ridge: "A" = the Azores Province (53–70°N), "B" = the Iceland Province (34–53°N) (Schilling and Sigurdsson 1979; Schilling et al. 1983). R = rock, G = glass

**Table 3.** Rare earth contents of Mohns and Knipovich Ridge basalts in ppm

| ID | La | Ce | Nd | Sm | Eu | Gd | Tb | Dy | Tm | Yb | Lu | $(La/Sm)_{EF}$ |
|---|---|---|---|---|---|---|---|---|---|---|---|---|
| EN 026 3D-1 | 60.9 | 130.4 | 50.5 | 9.61 | 2.91 | – | 1.32 | – | – | 2.40 | 0.39 | 4.44 |
| EN 026 3D-2 | 47.2 | 105.5 | 42.7 | 7.60 | 2.58 | – | 1.16 | – | – | 2.26 | 0.26 | 4.35 |
| EN 026 5D-1 | 31.9 | 69.7 | 29.5 | 5.84 | 2.04 | 8.0 | 1.14 | – | 0.47 | 2.70 | 0.36 | 3.82 |
| EN 026 5D-2 | 53.5 | 118.1 | 46.6 | 8.61 | 2.75 | 11.0 | 1.24 | – | – | 2.58 | 0.33 | 4.35 |
| EN 026 5D-3 | 36.6 | 80.3 | 30.5 | 5.89 | 2.00 | 7.3 | 0.91 | – | – | 2.27 | 0.30 | 4.35 |
| EN 026 4D-1 | 48.9 | 107.7 | 43.1 | 7.80 | 2.63 | 8.8 | 1.10 | – | – | 2.33 | 0.33 | 4.39 |
| EN 026 4D-2 | 59.8 | 132.2 | 52.3 | 9.33 | 2.94 | – | 1.36 | – | – | 2.73 | 0.36 | 4.49 |
| EN 026 4D-3 | 42.4 | 98.4 | 43.1 | 6.95 | 2.46 | 8.8 | 1.00 | – | – | 2.14 | 0.29 | 4.27 |
| EN 026 6D-1 | 30.8 | 60.6 | 22.3 | 4.61 | 1.63 | – | 0.84 | – | 0.35 | – | 0.25 | 4.68 |
| EN 026 2D-1 | 56.3 | 124.4 | 50.4 | 9.32 | 2.85 | – | 1.29 | – | – | 2.39 | 0.27 | 4.22 |
| EN 026 7D-1 | 9.5 | 24.2 | 13.0 | 3.51 | 1.34 | 5.4 | 0.77 | 4.4 | – | 2.80 | 0.37 | 1.90 |
| EN 026 7D-2 | 60.4 | 133.5 | 54.2 | 9.22 | 2.99 | 10.8 | 1.34 | – | – | 2.51 | 0.31 | 4.59 |
| EN 026 1D-1 | 58.7 | 134.4 | 54.1 | 9.25 | 3.14 | – | 1.50 | – | – | 2.74 | 0.34 | 4.44 |
| EN 026 1D-2 | 54.8 | 111.3 | 44.4 | 8.74 | 2.58 | 8.4 | 1.13 | – | – | 2.46 | 0.25 | 4.39 |
| EN 026 8D-1 | 18.9 | 43.3 | 23.8 | 6.24 | 2.15 | 8.9 | 1.33 | 8.3 | – | 4.29 | 0.58 | 2.12 |
| EN 026 8D-2 | 19.5 | 48.3 | 26.1 | 6.37 | 2.34 | 9.9 | 1.24 | – | 0.80 | 4.56 | 0.56 | 2.15 |
| EN 026 9D-1 | 10.8 | 25.5 | 15.2 | 3.77 | 1.49 | 5.3 | 0.86 | 5.7 | – | 2.84 | 0.41 | 2.01 |
| TR 139 30D-1 | 25.1 | 49.0 | 24.0 | 5.42 | 1.58 | – | 1.02 | – | – | 2.83 | 0.43 | 3.24 |
| TR 139 30D-2 | 25.1 | 52.9 | 25.2 | 5.68 | 1.70 | – | 1.26 | – | – | 3.85 | 0.45 | 3.09 |
| EN 026 10D-1 | 6.5 | 17.5 | 12.0 | 3.64 | 1.40 | – | 0.85 | 5.9 | – | 3.31 | 0.46 | 1.25 |
| EN 026 10D-2 | 8.0 | 16.7 | 11.6 | 4.27 | 1.15 | – | 0.86 | – | – | 3.22 | 0.40 | 1.30 |
| EN 026 11D-1 | 8.4 | 20.8 | 11.2 | 3.60 | 1.38 | – | 0.83 | – | – | 3.17 | 0.43 | 1.63 |
| TR 139 31D-1 | 5.2 | 13.3 | 11.9 | 3.70 | 1.38 | – | 0.91 | – | – | 3.36 | 0.48 | 0.98 |
| TR 139 31D-2 | 5.8 | 14.9 | 12.0 | 3.77 | 1.40 | – | 1.01 | – | – | 4.06 | 0.48 | 1.08 |
| EN 026 12D-2 | 13.8 | 29.0 | 13.1 | 3.27 | 1.30 | – | 0.73 | 4.8 | – | 2.43 | 0.34 | 2.95 |
| EN 026 12D-3 | 9.9 | 23.2 | 11.9 | 2.89 | 1.13 | – | 0.58 | – | – | 2.16 | 0.32 | 2.40 |
| TR 139 32D-1 | 5.7 | 14.5 | 10.9 | 3.18 | 1.08 | – | 0.81 | – | – | 3.09 | 0.42 | 1.25 |
| TR 139 32D-2 | 6.4 | 16.0 | 11.0 | 3.23 | 1.16 | – | 0.80 | – | – | 2.60 | 0.45 | 1.38 |
| EN 026 14D-1 | 3.0 | 9.1 | 6.6 | 2.58 | 1.42 | 4.7 | 0.67 | – | 0.42 | 2.55 | 0.35 | 0.83 |
| TR 139 33D-1 | 6.5 | 15.9 | 10.6 | 3.28 | 1.12 | – | 0.81 | – | – | 2.81 | 0.38 | 1.38 |
| TR 139 33D-2 | 5.7 | 14.7 | 10.7 | 3.34 | 1.06 | – | 0.77 | – | – | 2.99 | 0.38 | 1.20 |
| EN 026 15D-1 | 6.0 | 14.5 | 9.5 | 2.64 | 1.14 | 4.1 | 0.61 | – | – | 2.30 | 0.31 | 1.59 |
| EN 026 15D-2 | 6.9 | 15.1 | 10.3 | 3.39 | 0.98 | – | 0.65 | – | – | 2.59 | 0.40 | 1.43 |
| EN 026 16D-1 | 1.9 | 7.5 | 6.3 | 2.37 | 1.06 | 4.4 | 0.72 | 4.6 | – | 2.54 | 0.38 | 0.56 |
| EN 026 16D-2 | 2.2 | 8.8 | 7.6 | 2.55 | 1.16 | 4.8 | – | – | – | 2.77 | 0.34 | 0.60 |
| EN 026 32D-1 | 3.1 | 9.8 | 9.3 | 2.92 | 1.24 | 4.6 | 0.71 | – | 0.49 | 3.04 | 0.42 | 0.74 |
| EN 026 32D-3 | 3.5 | 8.7 | 7.5 | 3.29 | 1.02 | – | 0.70 | – | 0.45 | 3.06 | 0.39 | 0.74 |
| EN 026 31D-1 | 4.1 | 14.8 | 12.0 | 3.59 | 1.45 | 6.3 | 0.88 | – | 0.62 | 3.25 | 0.44 | 0.81 |
| EN 026 30D-1 | 6.5 | 15.2 | 10.0 | 3.11 | 1.25 | 4.4 | 0.72 | – | – | 2.43 | 0.37 | 1.47 |
| EN 026 29D-1 | 4.5 | 14.1 | 9.7 | 2.96 | 1.27 | – | 0.71 | – | 0.52 | 2.89 | 0.39 | 1.06 |
| EN 026 29D-2 | 5.3 | 12.9 | 9.9 | 3.59 | 1.04 | – | 0.76 | – | 0.50 | 2.80 | 0.39 | 1.03 |
| EN 026 27D-2 | 7.1 | 21.3 | 12.7 | 3.92 | 1.52 | 5.8 | 0.87 | – | 0.56 | 2.99 | 0.46 | 1.27 |
| EN 026 19D-1 | 6.6 | 17.8 | – | 3.42 | 1.39 | 5.3 | 0.69 | 5.2 | – | 2.62 | 0.35 | 1.36 |
| EN 026 21D-1 | 5.6 | 15.3 | 12.6 | 3.50 | 1.47 | 5.2 | 0.82 | 5.9 | 0.60 | 3.13 | 0.42 | 1.13 |
| EN 026 22D-1 | 6.5 | 18.3 | – | 3.25 | 1.34 | – | 0.79 | – | – | 2.64 | 0.40 | 1.40 |
| EN 026 22D-2 | 8.6 | 17.9 | 12.1 | 4.43 | 1.23 | – | 0.78 | – | – | 2.90 | 0.38 | 1.35 |
| EN 026 25D-1 | 6.6 | 17.1 | 11.9 | 3.54 | 1.37 | – | 0.75 | – | – | 2.63 | 0.36 | 1.30 |
| EN 026 25D-2 | 6.4 | 18.2 | 11.2 | 3.28 | 1.20 | – | 0.74 | – | – | 2.56 | 0.40 | 1.37 |
| JB-1 Standard[a] | 37.7 | 71.1 | 27.3 | 5.20 | 1.61 | 5.8 | 1.12 | – | 0.388 | 2.11 | 0.312 | |
| ±1 S.D. | 3.5 | 5.9 | 3.4 | 0.45 | 0.11 | 1.4 | 0.02 | – | 0.78 | 0.1 | 0.01 | |
| JB-1 Recommended[b] | 36.2 | 67.3 | 24.8 | 4.80 | 1.5 | 4.8 | 0.5 | – | – | 2.1 | 0.31 | |
| Chondrites[c] | 0.3 | 0.84 | 0.58 | 0.21 | 0.074 | 0.32 | 0.049 | 0.31 | 0.0351 | 0.18 | 0.025 | |

[a] Mean of three irradiations [b] JB-1 recommended values by Ando et al. (1974) [c] Average of 20 chondrites by Schmitt et al. (1964)

similar to those generally found in transitional regions between ocean islands and "normal" segments of the mid-ocean ridge system, such as the northern part of the Reykjanes Ridge, the Kolbeinsey Ridge (west of Jan Mayen) or the MAR south of the Azores and the Galapagos Ridge (Sigurdsson and Brown 1970; Campsie et al. 1973; Schilling 1973; Brooks and Jakobsson 1974; White and Schilling 1978; Schilling et al. 1983).

*Trace elements*

As anticipated from the $K_2O$ and $P_2O_5$ variations previously discussed, the REE patterns vary significantly along the Mohns-Knipovich Ridge. Basalts within a radius of 120 km from Jan Mayen exhibit high values of light-REE and steep chondrite-normalized patterns (Table 3, Fig. 5). This is true both for the "subaerial-looking" lavas and

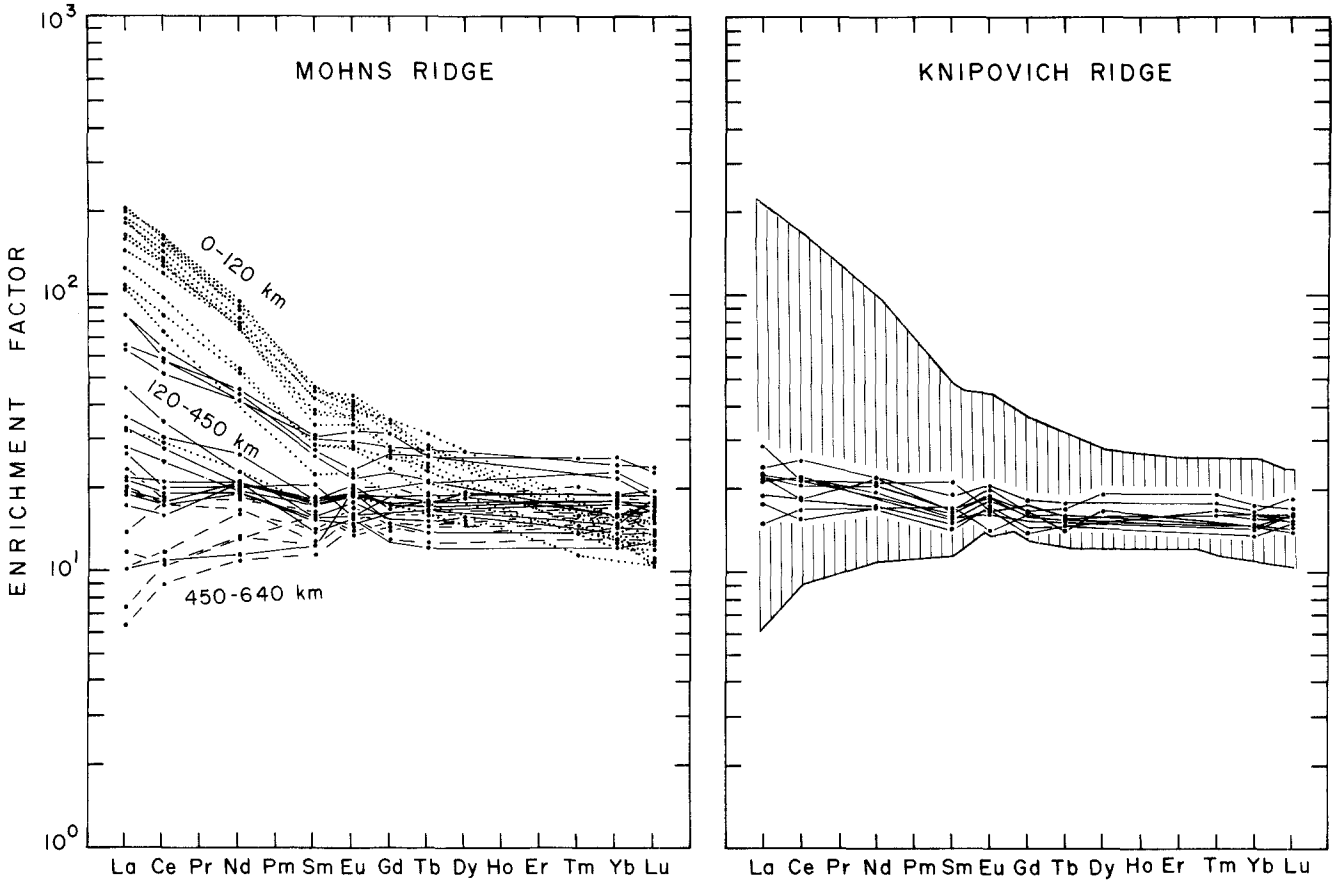


**Fig. 5.** Chondrite-normalized rare earth element (REE) patterns for the basalts studied. Distances given are distances from Jan Mayen. (0–120 km = dotted lines; 120–450 km = full lines; and 450–640 = dashed lines). The field covered by REE-patterns of Jan Mayen platform and Mohns Ridge rocks, is indicated by hatching in the right hand diagram

the pillow basalts from the JMP. With the exception of sample 7D-1, these rocks have $La_{EF}$ between 99 and 197, and $(La/Sm)_{EF}$ ratios in the range 3.8–4.7 ($X_{EF} = X_{sample}/X_{chondrite}$). The light-REE enrichment decreases eastwards along the Mohns Ridge to reach light-REE depleted patterns typical of normal-MORB on the EMR. However, on the KR the REE patterns are flat in the south and become slightly light-REE enriched northward ($La_{EF} = 14$–$27$, $(La/Sm)_{EF} = 1.0$–$1.8$). An important gradient is therefore apparent along the WMR, a minimum is reached on the EMR, and a weak gradient is present on the KR. Ratios of La to the other incompatible elements such as $P_2O_5$ and $K_2O$ measured in this study show similar changes along the profile (Fig. 6). The "subaerial-looking" JMP samples are more enriched in La and $K_2O$ relative to $P_2O_5$ ($K_2O/P_2O_5 = 4.25$; $P_2O_5/La = 106$) than are the EMR basalts and glasses ($K_2O/P_2O_5 = 1.40$; $P_2O_5/La = 321$), whereas basalts from the KR show intermediate values (Fig. 6).

Finally, latitudinal profiles similar to those of La/Sm have been observed for the variations in $^{87}Sr/^{86}Sr$, Rb/Sr, Ba/Sr, Rb/K and the inverse of $^{143}Nd/^{144}Nd$, on the basis of analyses made on the same samples by Wagonner et al. (1981) thus suggesting that the gradations observed must be derived from the source of these basalts in the upper mantle. However, on a relative basis, the incompatible element ratios tend to be more enriched over the JMP than are the strontium isotope ratios, probably as a result of lower degrees of partial melting of the high incompatible element and $^{87}Sr/^{86}Sr$ mantle source apparently present beneath the JMP.

## Petrography

The distinctions in major and trace element compositions between basalts erupted in different parts of the profile, are also apparent in the mineralogical nature and composition of the phenocrysts present in these rocks.

For example, most of the "subaerial-looking" rocks from the JMP (stations 2D, 3D, 4D, 1D-2, and 5D-2) are highly vesicular and have a high concentration of phenocrysts which may be up to a few millimeters in diameter. The phenocryst assemblage is olivine + plagioclase ± clinopyroxene ± magnetite. In contrast, most of the pillow lavas (1D-1, 5D-1, 5D-3, and all samples from station 6D and eastwards) have low concentrations of vesicles, and sparse small euhedral to subhedral phenocrysts. The phenocryst assemblage changes eastwards along the ridge to ± olivine ± plagioclase ± chrome spinel on the EMR and KR. Rocks with plagioclase as the only phenocryst are only observed on the KR. Cr-spinel often occurs as minute euhedral inclusions in olivine. Olivine frequently forms delicate skeletal euhedral crystals. The only deviation from this pattern is found at station 21D-1 on the KR. Fresh pillow basalt from this station is highly vesicular and has abundant phenocrysts of ol + plag + cpx + mt resembling the assemblage on the JMP although the bulk composition is hypersthene normative. Spinel is less frequently found on the EMR than further west and northeast.

The phenocryst assemblage ol + plag + Cr-spinel found in most samples from the EMR and KR, is typical of basalts extruded along the central part of "normal" mid-ocean ridge segments. Py-

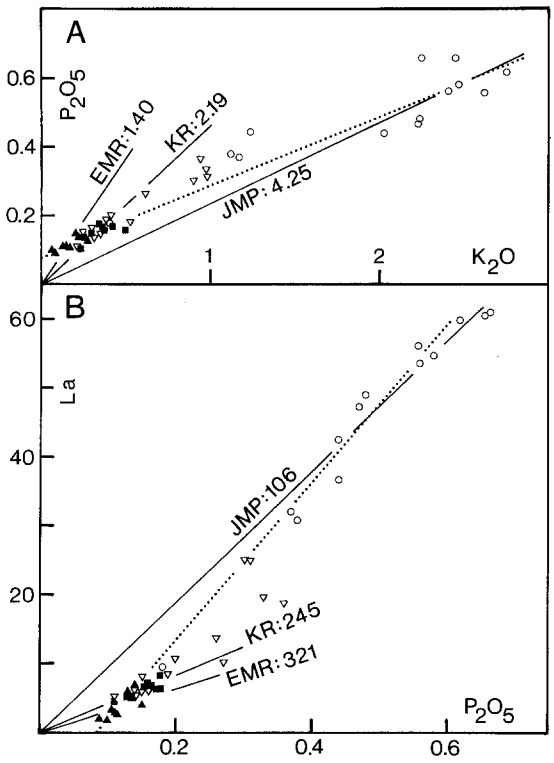


**Fig. 6A, B.** Plots of (A) wt.% $P_2O_5$ against wt.% $K_2O$, and (B) ppm La against wt.% $P_2O_5$. Open circles: Jan Mayen platform (JMP). Open triangles: Western Mohns Ridge (WMR). Filled triangles: Eastern Mohns Ridge (EMR). Filled squares: Knipovich Ridge (KR). Regression lines for different sample groups are represented by fully drawn lines. These lines also suggest fractional crystallization paths. Numbers represent the ratios $K_2O/P_2O_5$ (Fig. 6A) and $P_2O_5$/La (Fig. 6B). Dotted lines are possible magma mixing trends

roxene is rarely found in such rocks. Clinopyroxene is, however, frequently present along the transitional segment of the WMR. This is similar to what is observed on other transitional segments between islands (or shallow volcanic platforms) and normal ridge segments such as along the northern part of the Reykjanes Ridge, the Kolbeinsey Ridge, and south of the Azores (Dittmer et al. 1975; Schilling 1973; White and Schilling 1978; Schilling et al. 1983). As we will see later it is relevant to note that the abundance of clinopyroxene also tends to be higher in basalts erupted away from the ridge axis, and the presence of clinopyroxene and magnetite is frequently reported from basalts collected from the ocean floor by drilling (e.g. Frey et al. 1974; Hekinian et al. 1976; Melson et al. 1976; Wood et al. 1979).

## Phenocryst compositions

### *Olivine*

Olivine phenocrysts in samples collected on the JMP range in composition from $Fo_{70}$ to $Fo_{90}$ (Table 4) reflecting different degrees of evolution in these rocks. Sample 8D-1 from the WMR falls in this group. With one exception (21D-1), olivines in the fairly primitive samples from the rest of the Mohns-Knipovich Ridge have compositions between $Fo_{84}$ and $Fo_{88}$. Sample 21D-1, with a Mg-value of 0.62, however, contains $Fo_{70}$. Chemical zoning in olivine is weak or absent.

### *Plagioclase*

Plagioclase phenocrysts range from $An_{68}$ to $An_{89}$ and are frequently zoned (Table 4), normal and reverse zoning being equally common and found in all parts of the rift.

### *Pyroxene*

Most of the alkaline rocks collected on the JMP contain normally zoned phenocrysts of diopside to salite. $Al_2O_3$- and $TiO_2$-concentrations lie within the ranges 6.7–2.0 and 3.3–0.4 wt. percent respectively.

### *Spinel*

Two types of spinel have been observed in the basalt population studied (Table 5). Some of the "subaerial-looking" rocks from the JMR and sample 21D-1 from the KR contain a titaniferous magnetite with 5–6 weight percent $Al_2O_3$ and MgO. Other spinel-bearing basalts contain magnesiochromite. The titaniferous magnetites in basalts from the JMP fall within the range of compositions found by Haggerty (1976) to be characteristic of intraplate tholeiitic lavas. Similar compositions are also reported from magnetites in basalts drilled from the ocean floor (e.g. Clague et al. 1980). The magnesiochromites from the remaining Mohns-Knipovich Ridge have compositions similar to those found in olivine tholeiites from other parts of the Mid-Atlantic Ridge (Sigurdsson and Schilling 1976).

### *Temperatures*

Olivine-liquid equilibrium temperatures have been calculated on the basis of the distribution of MgO between olivine and glass, as calibrated by Bender et al. 1978 (Table 4). The crystallization temperatures range from 1,060 to 1,206° C. The lowest temperatures were obtained for glasses from dredge station 8D on the WMR. EMR samples give an average temperature of $1,191 \pm 9°$ C, KR glasses appear to have been quenched at slightly lower temperatures, $1,173 \pm 12°$ C.

## Discussion

Basalts dredged on the JMP are with minor exceptions of the alkalic kindred, whereas those from the Mohns-Knipovich Ridge are tholeiitic. More subtle petrological differences have also been pointed out between the tholeiites erupted on different segments of this ridge, but the differences between basalts from these segments are more obvious in their REE abundance patterns, incompatible element contents and their ratios, and Sr and Nd isotopic ratios.

Two important questions need to be further evaluated: (1) What is the provenance of the "subaerial-looking" basalts dredged on the JMP? (2) What are the causes of the petrological and geochemical distinctions noted between basalts erupted on WMR, the EMR, the KR, and the JMP (if in situ)?

### *Provenance of the dredged basalts from the Jan Mayen Platform*

The "subaerial-looking" alkali basalts could have the following provenance:

**Table 4.** Olivine and plagioclase compositions (in mole percent endmembers), and temperatures calculated on the basis of the distribution of MgO between olivine and glass (Bender et al. 1978)

| | Olivine | | Plagioclase | | | | | | T°C |
|---|---|---|---|---|---|---|---|---|---|
| | CORE | RIM | CORE | | | RIM | | | |
| | Fo | Fo | An | Ab | Or | An | Ab | Or | |
| EN 026 2D-1R | 74.3 | 73.4 | 79.2 | 19.1 | 1.8 | 80.7 | 18.0 | 1.3 | |
| EN 026 1D-1R | 70.2 | | 84.1 | 14.8 | 1.0 | | | | |
| EN 026 1D-1G | 81.4 | 80.7 | 73.9 | 25.9 | 0.2 | 75.0 | 25.0 | 0.1 | 1174 |
| EN 026 4D-1R | 90.0 | | 84.1 | 14.4 | 0.7 | 51.1 | 44.4 | 4.6 | |
| EN 026 5D-1R | 89.8 | 80.7 | 70.2 | 28.4 | 1.4 | 68.3 | 30.3 | 1.4 | |
| EN 026 5D-2R | 75.9 | | 81.5 | 17.3 | 1.2 | 85.7 | 13.2 | 1.1 | |
| EN 026 6D-1R | 89.6 | 86.4 | 87.2 | 12.4 | 0.4 | 81.7 | 17.6 | 0.8 | |
| EN 026 7D-1G | 85.2 | | | | | | | | 1191 |
| EN 026 7D-2R | 88.2 | 72.5 | 88.3 | 11.0 | 0.8 | 77.9 | 22.1 | 0.1 | |
| EN 026 8D-1R | 77.1 | 71.7 | 66.3 | 33.0 | 0.7 | 67.7 | 20.9 | 0.5 | |
| EN 026 8D-1G | 70.4 | | 64.6 | 34.5 | 0.9 | | | | 1060 |
| EN 026 8D-2G | 70.4 | | 67.3 | 31.9 | 0.3 | 65.7 | 33.0 | 0.5 | 1068 |
| EN 026 9D-1G | 85.4 | | 73.8 | 25.8 | 0.4 | | | | 1179 |
| EN 026 30D-2G | 87.5 | 86.6 | 73.6 | 25.8 | 0.6 | 71.9 | 27.3 | 0.8 | 1178 |
| EN 026 10D-1G | 84.9 | | 73.0 | 26.8 | 0.3 | | | | 1181 |
| EN 026 11D-1G | 83.5 | | 72.5 | 27.4 | 0.1 | | | | 1186 |
| TR 139 31D-1G | 85.2 | | 76.4 | 23.5 | 0.1 | | | | 1188 |
| TR 139 31D-2G | 85.1 | | 78.4 | 21.4 | 0.2 | 72.4 | 27.5 | 0.1 | 1183 |
| EN 026 12D-2G | 86.3 | | 83.7 | 15.9 | 0.4 | | | | 1173 |
| TR 139 32D-1G | 87.1 | | | | | | | | 1198 |
| TR 139 32D-2G | 84.7 | | 81.9 | 18.1 | 0.0 | 83.6 | 16.3 | 0.1 | 1169 |
| EN 026 14D-1G | 85.1 | | 85.2 | 14.6 | 0.2 | 71.9 | 27.9 | 0.2 | 1182 |
| TR 139 33D-1R | 86.1 | | 71.9 | 27.9 | 0.3 | | | | |
| EN 026 15D-1G | 87.8 | 87.0 | 73.1 | 26.5 | 0.4 | | | | 1189 |
| EN 026 15D-2G | 86.1 | | | | | | | | 1183 |
| EN 026 16D-1G | 86.6 | | 83.1 | 16.5 | 0.1 | | | | 1196 |
| EN 026 32D-1G | 86.0 | | 89.4 | 10.6 | 0.0 | 69.5 | 30.5 | 0.0 | 1206 |
| EN 026 32D-3G | 85.0 | | 80.5 | 19.4 | 0.1 | 85.2 | 14.7 | 0.1 | 1200 |
| EN 026 31D-1G | 85.7 | | 72.8 | 26.9 | 0.3 | 68.4 | 31.4 | 0.2 | 1184 |
| EN 026 30D-1G | 86.5 | | | | | | | | 1185 |
| EN 026 29D-1G | 87.1 | | 76.8 | 23.0 | 0.2 | | | | 1193 |
| EN 026 29D-2G | | | 76.1 | 23.7 | 0.2 | | | | |
| EN 026 27D-2R | 84.9 | | 76.9 | 23.1 | 0.1 | 69.0 | 30.5 | 0.5 | |
| EN 026 19D-1G | 87.7 | | 71.5 | 28.2 | 0.3 | | | | 1173 |
| EN 026 21D-1R | 69.8 | 69.2 | 82.1 | 16.6 | 1.4 | 72.0 | 25.4 | 2.6 | |
| EN 026 21D-1G | 84.7 | | 72.2 | 27.6 | 0.3 | | | | 1175 |
| EN 026 22D-1G | 87.2 | 86.8 | 70.8 | 28.9 | 0.3 | 74.2 | 25.7 | 0.1 | 1161 |
| EN 026 22D-2G | 86.7 | | 73.2 | 27.2 | 0.5 | | | | 1159 |
| EN 026 25D-1G | 88.0 | 86.5 | 71.1 | 28.6 | 0.3 | | | | 1168 |
| EN 026 25D-2G | | | 80.0 | 19.6 | 0.4 | | | | |

**Table 5.** Compositions of magnetites and Cr-spinels (weight percent)

| | EN 026 1D-1 | EN 026 4D-2 | EN 026 5D-2 | EN 026 6D-1 | | TR 139 32D-1 | TR 139 33D-1 | EN 026 27D-2 | EN 026 19D-1 | | EN 026 21D-1 | EN 026 22D-1 | EN 026 22D-2 | EN 026 25D-1 |
|---|---|---|---|---|---|---|---|---|---|---|---|---|---|---|
| $SiO_2$ | 0.26 | 0.32 | 0.27 | 0.23 | 0.27 | 0.22 | 0.39 | 0.27 | 0.27 | 0.22 | 0.28 | 0.47 | 0.32 | 0.39 |
| $TiO_2$ | 3.74 | 0.83 | 17.08 | 1.25 | 0.87 | 0.87 | 0.81 | 1.34 | 0.63 | 0.94 | 24.15 | 0.82 | 0.83 | 1.09 |
| $Al_2O_3$ | 7.68 | 23.47 | 6.20 | 21.80 | 29.07 | 23.35 | 22.31 | 22.75 | 28.04 | 25.63 | 4.74 | 23.78 | 24.66 | 21.29 |
| $Cr_2O_3$ | 0.08 | 39.48 | 0.17 | 42.03 | 35.17 | 38.58 | 39.29 | 39.91 | 38.00 | 39.25 | 0.27 | 38.42 | 38.63 | 38.81 |
| $Fe_2O_3$ | 54.22 | 6.69 | 31.11 | 5.47 | 6.68 | 7.47 | 7.41 | 5.79 | 5.23 | 6.38 | 17.61 | 6.21 | 7.32 | 6.62 |
| FeO | 28.15 | 14.99 | 38.39 | 12.90 | 12.32 | 13.99 | 15.31 | 16.88 | 13.68 | 14.34 | 45.08 | 15.24 | 13.56 | 15.35 |
| MnO | 0.40 | 0.32 | 0.41 | 0.16 | 0.54 | 0.12 | 0.47 | 0.36 | 0.40 | 0.09 | 0.36 | 0.29 | 0.25 | 0.07 |
| MgO | 4.81 | 14.05 | 6.13 | 15.39 | 16.53 | 14.59 | 13.54 | 13.01 | 15.46 | 15.20 | 5.58 | 13.71 | 14.27 | 13.21 |
| CaO | 0.05 | 0.09 | 0.06 | 0.00 | 0.00 | 0.02 | 0.08 | 0.10 | 0.17 | 0.14 | 0.08 | 0.27 | 0.07 | 0.20 |
| | 99.39 | 100.24 | 99.82 | 99.23 | 101.45 | 99.21 | 99.61 | 100.41 | 101.87 | 102.19 | 98.14 | 99.21 | 100.01 | 97.02 |

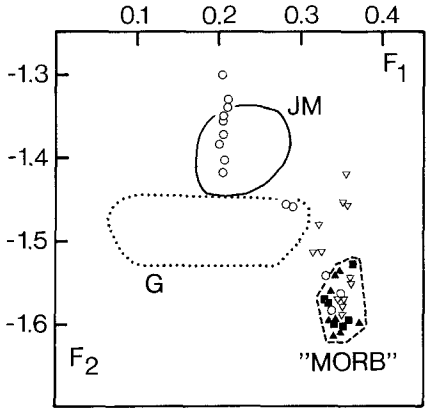


**Fig. 7.** Comparison between samples of the present study, and fields occupied by Tertiary to recent basaltic rocks from Jan Mayen (JM) (solid line) (data from Imsland, 1980) and southeast Greenland (G) (dotted line) (data from Nielsen, 1978), using discriminant functions ($F_1$ and $F_2$) defined by Pearce (1976). Open circles: Jan Mayen platform (JMP). Open triangles: Western Mohns Ridge (WMR). Filled triangles: Eastern Mohns Ridge (EMR). Filled squares: Knipovich Ridge (KR). "MORB" field includes EMR and KR (dashed line)

(1a) They were erupted subaerially and essentially are in place where dredged. Subsequent subsidence (and sea level rise) submerged the volcanoes and the platform to their present depth, a feature we have commonly observed on the Iceland Insular Platform (e.g. McMaster et al. 1977). In this case the rounded samples would have been eroded during beach processes.

(1b) The basalts belong to the Jan Mayen Island volcanic complex and were transported to their dredged location either as ejecta or landslides (angular samples) or by mudflow or ice (rounded samples).

(2) The rocks are foreign to the JMP and represent ice-rafted material of unknown provenance, but most likely from the Tertiary Volcanic Province of East Greenland, judging from present ice movements in the Norwegian-Greenland Sea.

Volcanic rocks from the Jan Mayen Island are potassic, alkaline and range from ankaramites through alkali basalt to trachytes (Imsland 1980). Representative alkali basalts have $La_{EF}$ between 3.2 and 4.7 (Goles 1975) and $^{87}Sr/^{86}Sr$ ratios of $0.7034 \pm 4$ (O'Nions and Pankhurst 1974).

The Tertiary Volcanic Province of East Greenland is dominated by quartz-normative flood basalts with less than 0.5 wt.% $K_2O$, and $K_2O/Na_2O < 0.12$ (Fawcett et al. 1973). The associated dike swarms, however, include alkaline mafic dikes with 2.6 to 15.1% normative nepheline, and $K_2O/Na_2O$ ratios between 0.4 and 1.3 (Nielsen 1978).

The above summary indicates that both the Jan Mayen and the Tertiary East Greenland Volcanic Province offer magmatic products with major element compositions which at first glance resemble the "subaerial-looking" basalts dredged on the JMP. We can evaluate the probable provenance of the dredged JMP alkali basalts by discriminant analysis. Pearce (1976) has shown that the functions $F_1$ ($=0.88\ SiO_2 - 0.0774\ TiO_2 + 0.0102\ Al_2O_3 + 0.0066\ FeO - 0.0017\ MgO - 0.0143\ CaO - 0.0155\ Na_2O - 0.0007\ K_2O$) and $F_2$ ($=0.013\ SiO_2 - 0.0185\ TiO_2 - 0.0129\ Al_2O_3 - 0.0134\ FeO - 0.03\ MgO - 0.0204\ CaO - 0.0481\ Na_2O + 0.0715\ K_2O$) have proven effective in separating basalts from different tectonic settings. We have included as data points all the dredged rocks from the Jan Mayen-Knipovich Ridge profile with $SiO_2$ and MgO contents in the range between 44 and 52, and 4 and 11 wt.%, respectively. For basalts from the Tertiary East Greenland Province (Nielsen 1978) we have disregarded the potassium-poor flood basalts which clearly differ from the JMP samples.

Figure 7 shows that the rocks of "subaerial" appearance and the pillow basalts 1D-1 and 7D-2 from the JMP define a group with high $F_2$ and relatively low $F_1$ values which overlaps with the field of the Jan Mayen island basalts. Glasses from the EMR and KR define another group (MORB) with relatively high $F_1$ and $F_2$ values. The rest of the pillow basalts, including 5D-1, 5D-3, and 6D-1, fall between the two groups, or in the MORB-field (including 7D-1). Observations from Fig. 7 thus lend support to a provenance described under (1a) and (1b) above for the alkali basalts dredged on the JMP, and furthermore suggest that the alkali volcanism is not restricted to the island itself but is fairly representative of the entire platform. This is also evident from the comparison of the few REE analyses (Weigand et al. 1972) and Sr isotope determinations available for the Jan Mayen alkali basalts (O'Nions and Pankhurst 1974; Lussiaa and Vidal 1973), the basalts we dredged on the platform (this study and Wagonner et al. 1981), and others previously reported by Pedersen et al. (1976).

*Some possible origins of the latitudinal variations*

Several geological factors appear to be responsible for the petrological and geochemical variations revealed from this study along the Jan Mayen-Mohns-Knipovich Ridge profile. These include mantle heterogeneities, partial melting conditions, fractional crystallization during magma ascent and emplacement into the crust, diffusion-controlled phenomena in magma chambers, such as the Soret effect, and the fact that these processes are not likely to have taken place at the same depth (pressure). Mixing between distinct reservoirs at different magmatic stages and depths, extending down to the uppermost mantle, is also likely to have taken place. The extent of these processes is now evaluated on the basis of the data accumulated in this study.

*Mantle heterogeneities.* We have pointed out that the similarity in the variation along the JMP-WMR-EMR-KR profile of La/Sm and $^{87}Sr/^{86}Sr$, and the inverse variation for $^{143}Nd/^{144}Nd$ (Wagonner et al. 1981), strongly suggest that mantle heterogeneities are present beneath this region. This is also readily apparent in Fig. 8a which shows the variation of $(La/Sm)_{EF}$ versus $Mg/(Mg+Fe^{2+})$ for the dredged basalts, on which we have superimposed a model of partial melting for a single mantle source followed by variable extent of fractional crystallization. The model calculations are based on the method of Shaw (1970), Greenland (1970), and Irvine (1977a and b). The mantle source was assumed to be a peridotite with a light-REE depleted pattern ($La/Sm_{EF} = 0.5$) likely to be representative of the source of normal MORB. Further details of the two models are given in the caption of Fig. 8. It is evident that the $(La/Sm)_{EF}$ variations over the range of high Mg-values which are probably representative of more primitive melts, exceeds significantly the maximum fractionation that could be produced over the range 0 to 100% melting of such a single, light-REE depleted mantle source, or by mixing between such

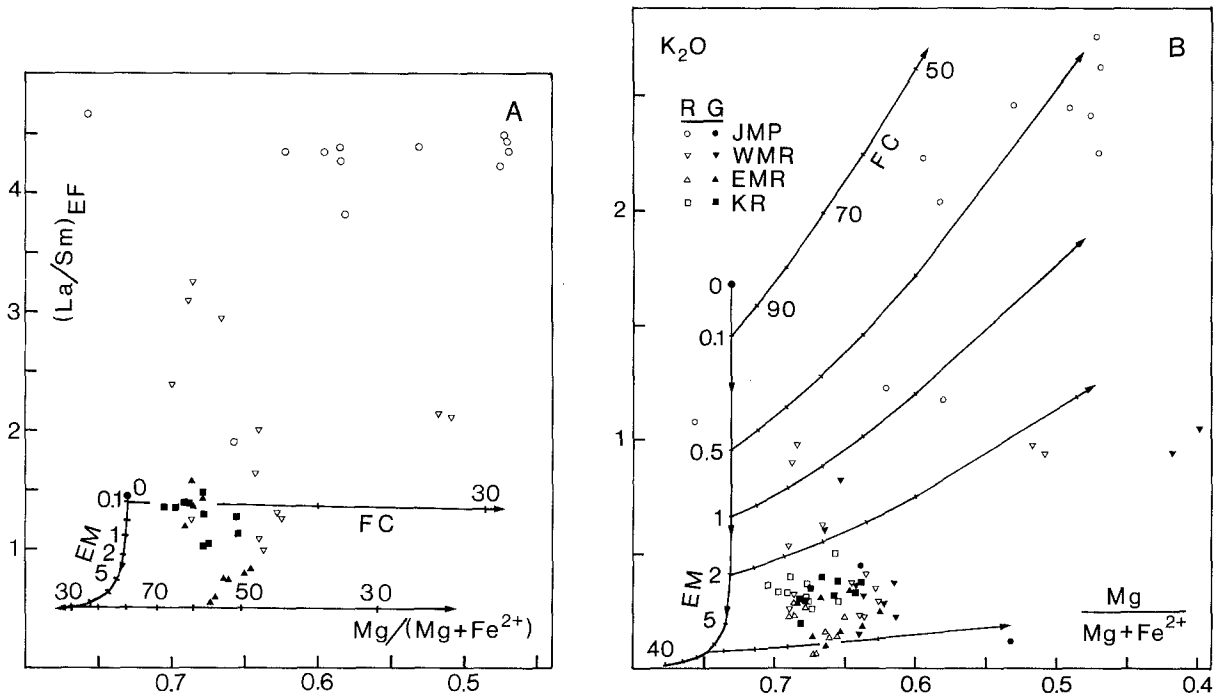


**Fig. 8A, B.** Plots of $(La/Sm)_{EF}$ (A) and $K_2O$ (B) against $Mg/(Mg+Fe^{2+})$ (cation proportions, $Fe^{3+}/(Fe^{2+}+Fe^{3+})=0.15$). Mohns-Knipovich data are compared with calculated evolution trends representative of progressive fractional removal (FC) of $ol_{28}plag_{72}$ from basaltic melts derived by different degrees of equilibrium melting (EM) of a peridotite mantle source. We have assumed equilibrium melting of a "eutectic" basalt composition $ol_{16}cpx_{21}opx_{10}plag_{53}$ from a spinel lherzolite mantle ($ol_{66}cpx_8opx_{24}sp_2$).Similar results are obtained if the assumed mantle composition is $ol_{63}cpx_2opx_{30}$ $gar_5$. These compositions are in agreement with (a) experimental data by Mysen and Boettcher (1975a, b) and Presnall et al. (1978, 1979); (b) estimated mantle composition from means of lherzolite nodule chemistry (Maaloe and Aoki 1977); and (c) means of analyses of the most mafic MOR basalts (Bryan and Moore 1977; Langmuir et al. 1977). Partition coefficients used are for ol/melt: 0.009 (La), 0.015 (Sm), 0.0056 (K); for cpx/melt: 0.14 (La), 0.5 (Sm), 0.002 (K); for opx/melt: 0.0055 (La), 0.012 (Sm), 0.009 (K); for plag/melt: 0.11 (La), 0.06 (Sm), 0.2 (K), and for spinel/melt: 0.0005 (Ls), 0.001 (Sm), 0.0001 (K) (Arth 1976; Frey et al. 1978; Irving 1978; Stosch 1982). Numbers indicate percent melt. Abreviations as in Fig. 7

melts. Models with other choices of mineral assemblages for the mantle source and other partition coefficients are unlikely to change this conclusion, unless unrealistically high contents of garnet in the peridotite mantle residue are assumed.

The data suggest that the mantle underlying the JMP region is enriched in light-REE, K, and other incompatible elements. The Sr and Nd isotope systematics furthermore suggest that such enrichment must be at least as old as several hundred millions of years (Waggoner et al. 1981, and pers. comm.). What is also necessary is to determine whether the incompatible element gradations observed along the MAR northeastward of the JMP (Fig. 3): (1) reflect similar variations in the mantle source of basalts beneath the profile; or (2) are due to some mixing processes and reflect the dynamics of mantle advection and of magma emplacement into the crust along the MAR axis; or (3) towards the JMP the melts are derived from progressively greater dephts in a vertically zoned mantle. Further consideration of these questions will be dealt with in greater detail in another paper discussing Sr and Nd systematics of these rocks (Waggoner and Schilling in prep.). However, Fig. 8. shows that if mixing of melts is involved, it must have taken place between heterogeneous end members and be rather complex. The possibility that a mantle plume is rising beneath the JMP and that some of this material mixes along the ridge remains a viable explanation for the steep downgradient in La/Sm and other incompatible elements observed along the Mohns Ridge. The model does, however, require further testing. The slight northward increase in incompatible element ratios on the KR (and $^{87}Sr/^{86}Sr$ etc. reported by Waggoner et al. 1981) further requires either that another plume is present north of the limit of the profile and induces a southward subaxial flow, or that the mantle beneath the region is compositionally very slightly gradational for some other reason.

It is also evident that the northward decrease in the spreading rate of the MAR in the region cannot be evoked as an explanation for the gradational variation in the LILE element ratios because of the minimum they go through at the intersection of the EMR with the KR; nor would spreading rate variations explain the Sr and Nd isotope gradation observed by Waggoner et al. (1981), since these isotope ratios do not respond to variation in degrees of partial melting (e.g., Hanson 1977).

*Partial melting.* Figure 8 suggests that the enriched nature of basalts dredged on the JMP may in part reflect a smaller degree of partial melting of the mantle source beneath the Platform than of that underlying the EMR. It is, however, difficult to ascertain to what extent the enrichments in light-REE and other incompatible elements near Jan Mayen should be attributed to smaller degrees of melting, and to what extent they are due to enrichment of the underlying mantle source.

Also likely to contribute to the alkali nature of the ba-

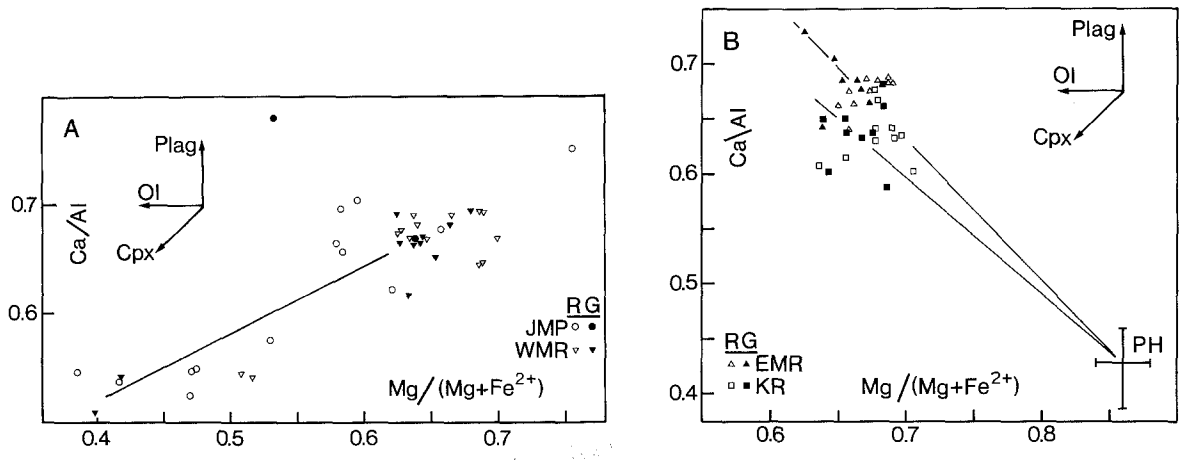


**Fig. 9A, B.** Relations between Ca/Al and Mg/(Mg+$Fe^{2+}$) (cation proportions) among Mohns-Knipovich Ridge samples. JMP: Jan Mayen Platform, WMR: Western Mohns Ridge, EMR: Eastern Mohns Ridge, KR: Knipovich Ridge, R: rock, G: glass, PH: means of coexisting olivine and plagioclase phenocrysts

**Table 6.** Representative petrographic mixing calculations, together with estimated differences between quench temperature of parent ($T_P$) and daughter ($T_D$). F = proportion of melt

| | Western Mohns Ridge | | | Eastern Mohns Ridge | | Knipovich Ridge | |
|---|---|---|---|---|---|---|---|
| Parent | TR 32D-1 | TR 32D-1 | EN 10D-1 | EN 32D-1 | EN 32D-1 | EN 19D-1 | EN 29D-1 |
| Daughter | TR 32D-2 | EN 10D-1 | EN 8D-1 | EN 15D-1 | EN 14D-1 | EN 22D-1 | EN 29D-2 |
| Ol % | −29 | −23 | −13 | −26 | −31 | −30 | −25 |
| Plag % | −53 | −56 | −53 | −74 | −69 | −70 | −75 |
| Cpx % | −18 | −21 | −34 | | | | |
| F | 0.87±0.12 | 0.87±0.08 | 0.55±0.17 | 0.9±0.2 | 0.90±0.15 | 0.95±0.13 | 0.95±0.04 |
| $T_P$−$T_D$ (°C) | 29 | 17 | 119 | 17 | 24 | 12 | |

salts dredged on the JMP and for that matter those of Jan Mayen as well, is the possibility that this volcanism is not entirely associated with the MAR ridge itself, but is off-axis in nature, where geothermal gradients are likely to be lower and the mantle solidus exceeded at greater depths (e.g. Aumento 1968). As previously noted, the presence of abundant clinopyroxene phenocrysts in the alkali basalts of the JMP is also consistent with off-ridge type of volcanism, and so are the compositions of the titanomagnetites found in these rocks.

The fact that the heavy-REE contents of the alkali basalts from the JMP tend to be slightly lower than those of the tholeiites from the EMR-KR, thus resulting in crossover REE patterns in the heavy-REE end (Fig. 5), suggests that garnet was a residual phase during partial melting and generation of the alkali basalts from the platform (see e.g. Schilling 1976). The fact that the JMP basalts are lower in $SiO_2$ content is consistent with melting under higher pressure conditions (e.g. Mysen and Kushiro 1977). Various authors have suggested that the most primitive alkaline basalts from the Jan Mayen island were probably formed in the depth range of 35 to 70 km (Weigand 1972; Weigand et al. 1972; O'Nions and Pankhurst 1974); and more recently Imsland (1980) has shown that the mafic ankaramites from the island were probably derived at pressures greater than 18 Kb (>60 km), within or below the field of stability of spinel.

*Fractional crystallization.* Most rocks and glasses represent three-phase equilibria (melt+ol+plag) and have Mg/(Mg+$Fe^{2+}$) ratios below those of the most primitive glasses collected along the MAR (0.70–0.72, Bender et al. 1978), suggesting that they have been subjected to some degree of fractional crystallization at low pressure. Major element variations observed within each geographic group of basalts may be due to different degrees of fractional crystallization. We have tested this suggestion by petrological modelling on the basis of major element analyses of glasses and phenocrysts, using the phenocryst assemblages we have observed in the different groups. In each calculation the data set of each phase is normalized relative to that of the glass assumed to represent "parent magma", and each oxide is weighted according to analytical precision. The results are listed in Table 6, and shown graphically in Fig. 9. This shows that removal of different mineral assemblages must be invoked for the basalts from the EMR-KR and for those from the JMP-WMR. Removal of pyroxene is needed to account for the decrease in Ca/Al ratios with decreasing Mg-value of the basalts located on or in the vicinity of the JMP. This is in good agreement with the phenocryst assemblages observed in these different groups.

The phase assemblage in the WMR basalts of ol+plag±cpx±mt. Petrological modelling was therefore attempted assuming removal of: (1) ol+plag+cpx, or (2) ol+plag. In general assumption (2) gave large deviations between "observed" and "estimated" daughter compositions, whereas assumption (1) gave relatively small deviations for some parent-daughter combinations, suggesting an average crystal proportion in the extract of

$ol_{19}plag_{52}cpx_{29}$ in the vicinity of the JMP (Table 6). About 50 percent crystals would have to be removed from a liquid with composition similar to that of the most primitive glass, in order to produce the most evolved rocks.

Petrological modelling of the EMR and KR glasses implies that the observed major element variations may be partly explained by removal of olivine and plagioclase in the proportion 28:72 (Table 6, Fig. 9). The calculated proportion between olivine and plagioclase in the hypothetical crystal extract is in excellent agreement with experimental data which indicate that tangents to the olivine-plagioclase liquidus boundary at low pressure will intersect the ol-plag join at approximately $ol_{30}plag_{70}$ (Cox and Bell 1972; Presnall et al. 1978). These basalts seem to have erupted at very similar stages of evolution, perhaps suggesting that the magmachambers underlying the EMR are at a quasi steady-state of magma output and supply. The petrological modelling indicates that it would take a removal of less than 20 percent crystals to produce the most evolved glass in the two groups EMR and KR, from the least evolved ones, if fractional crystallization only is invoked.

Fractional crystallization paths shown in Fig. 8 for the EMR-KR group were calculated on the basis of removal of a phase assemblage composed of $ol_{28}plag_{72}$, as determined by petrological modelling. Within each group of basalts, the glasses show an excellent agreement between stage of evolution, as indicated by petrological modelling and position in Fig. 8, and estimated quench temperature (Tables 4, 6). The appearance of clinopyroxene and, in some extreme cases, magnetite, in rocks from the JMP and EMP where fractional crystallization appears to have been most extensive, agree with experimentally determined low pressure crystallization paths for such basalts (see e.g. Walker et al. 1979). This agreement lends additional support to the conclusion that the observed compositional variations partly reflect different degrees of fractional crystallization.

The tendency for lower Ca/Al ratios and quench temperatures at a given Mg-value for the KR basalts relative to those from EMR may imply that some pyroxene has crystallized at greater depth and been removed from the Knipovich melts prior to their quenching. Alternatively these differences may reflect systematic major element differences between KR and EMR primary melts. Finally, we emphasize that the observed chemical variations cannot merely be explained by fractional crystallization alone or mixing between cosanguineous primitive and evolved melts.

*Soret separation.* Recent experiments by Walker and DeLong (1981) suggest that Soret separation may produce chemical differentiation in a magma-chamber. We have therefore considered diffusion as a possible explanation for the chemical distinction between KR and EMR glasses. However, the behaviour of Ti differs from that predicted by Walker and DeLong's experiments and it must be concluded that Soret separation did not play any important role in the genesis of these glasses.

## Conclusions

Significant differences in the bulk composition, type of phenocrysts and their compositions, and incompatible trace element contents of basalts erupted along the JMP – WMR –EMR – KR profile suggest the following conclusions:

(1) Dredged basalts from the JMP are strongly enriched in light-REE and other incompatible elements and have high $^{87}Sr/^{86}Sr$ and low $^{143}Nd/^{144}Nd$ ratios. These dredged basalts are indistinguishable from alkali basalts from Jan Mayen Island. These appear to have segregated from greater depth by smaller degrees of melting of a mantle source significantly enriched in light-REE relative to chondrites and to the mantle source underlying the EMR. These results suggest that alkali volcanism on the JMP is not merely confined to the island itself but is more widespread than so far realized, and likely to be off-ridge in type as well.

(2) Basalts from the EMR are tholeiitic, light-REE depleted, low in $^{87}Sr/^{86}Sr$ and high in $^{143}Nd/^{144}Nd$. They appear to have been derived from a mantle source depleted in light-REE relative to chondrites, and low in other incompatible elements. Petrologically and geochemically the Jan Mayen Province resembles that of the Azores rather than Iceland.

(3) Basalts from the WMR have petrologic and geochemical characters that are intermediate between those erupted on the JMP and EMR. The incompatible element concentrations and $^{87}Sr/^{86}Sr$ ratios decrease fairly rapidly northward along this part of the Mohns Ridge, as does elevation. It remains uncertain whether such gradation reflects: (a) similar gradation in the mantle underlying this part of the MAR ridge, (b) mixing between distinct reservoirs such as the binary mantle plume – LILE-depleted asthenosphere model previously proposed for Iceland by Schilling (1973) and Schilling et al. (1983), or (c) vertical gradation in the mantle with incompatible elements and $^{87}Sr/^{86}Sr$ increasing with depth, the melts being derived from progressively greater depths towards the JMP.

(4) Basalts from the KR are generally tholeiitic and petrologically resemble those from the EMR. However, they are slightly enriched in light-REE relative to chondrites. In general the KR basalts also have higher incompatible element contents and Sr isotope ratios, and lower Nd isotope ratios than those from the EMR, and their enrichments increase very slightly northward. The cause of this geochemical gradient remains unknown, but could suggest another mantle plume north of 77°30′N.

(5) Petrological and geochemical modelling suggests that the diversities of melt compositions observed locally can be explained by fractional crystallization dominated by olivine + plagioclase + clinopyroxene ± magnetite on and in the vicinity of the JMP, whereas over the EMR and KR it is dominated primarily by olivine + plagioclase ± spinel. The possibility that some of the local variations on the EMR and KR could be attributed to Soret separation was tested. Fractionation patterns in complete agreement with such diffusion controlled phenomena were not detected, suggesting that the Soret effect did not play any significant role in this particular case.

*Acknowledgements.* We thank B.H. Baker and T.N. Irvine for discussions on the effect of diffusion in magma-chambers, and P. Vogt for unpublished magnetic data and maps of the Knipovich Ridge region. We are also grateful to Captain H.P. Bennet and his crew for sailing safely and enthusiastically around icebergs up to the edge of the Northern sea-ice. We thank F. DiMeglio and staff at RINSC for neutron irradiations and facilities. This work was partly supported by NSF grant OCE78-24690.

## References


Ando A, Kurasawa T, Ohmori T, Takeda E (1974) Compilation of data on the GSJ geochemical reference sample JG-1 granodiorite and JB-1 basalt. Geochim J 8:175–192

Arth JC (1976) Behavior of trace elements during magmatic processes – a summary of theoretical models and their applications. J Res US Geol Surv 4:41–47

Aumento F (1968) The Mid-Atlantic Ridge near 45°N, II. Basalts from the area of Confedereration Peak. Can J Earth Sci 5:1–21

Bender JF, Hodges FN, Bence AE (1978) Petrogenesis of basalts from the project FAMOUS area: experimental study from 0 to 15 kbars. Earth Planet Sci Lett 41:277–302

Brooks CK, Jakobsson SP (1974) Petrochemistry of the volcanic rocks of the North Atlantic Ridge system. In: Kristiansson L (ed) Geodynamics of Iceland and the North Atlantic area. D Reidel, Dordrecht, 139–154

Campsie J, Bailey JC, Dittmer F (1973) Chemistry of tholeiites from the Reykjanes Ridge and Charlie Gibbs Fracture Zone. Nature Phys Sci 244:71–73

Clague DA, Fish MR, Bence AE (1980) Mineral chemistry of basalts from Ojin, Nintoku, and Suiko Seamounts, leg 55 DSDP. Initial Reports of the Deep Sea Drilling Project, vol 55, pp 607–637

Cox KG, Bell JD (1972) A crystal fractionation model for basaltic rocks of the New Georgia Group, British Solmon Islands. Contrib Mineral Petrol 37:1–13

Dittmer F, Fine S, Rasmussen M, Bailey JC, Campsie J (1975) Dredged basalts from the mid-ocean ridge north of Iceland. Nature 254:298–301

Fawcett JJ, Brooks CK, Rucklidge JC, Gasparrini EL (1973) Chemical petrology of Tertiary flood basalts from the Scoresby Sund area. Meddr Grønland Bd 195, Nr 6:1–54

Feden RH, Vogt PR, Fleming HS (1979) Magnetic and bathymetric evidence for the "Yermak hot spot" northwest of Svalbard in the Arctic Basin. Earth Planet Sci Lett 44:18–38

Frey FA, Bryan WB, Thompson G (1974) Atlantic Ocean floor: geochemistry and petrology of basalts from Legs 2 and 3 of the Deep Sea Drilling Project. J Geophys Res 79:5507–5527

Frey FA, Green DH, Roy SD (1978) Integrated models of basalt petrogenesis: a study of quartz tholeiites to olivine melilitites from South Eastern Australia utilizing geochemical and experimental petrological data. J Petrol 19:463–513

Goles GG (1975) Basalts of unusual composition from the Chyulu Hills, Kenya Lithos 8:47–58

Greenland LP (1970) An equation for trace element distribution during magmatic crystallization. Am Mineral 55:455–465

Haggerty SE (1976) Opaque mineral oxides in terrestrial igneous rocks. In: Rumble III D (ed) Oxide Minerals, Mineral Soc Am Short Course Notes, vol 3, ppHg-101–300

Hanson GN (1977) Geochemical evolution of the suboceanic mantle. J Geol Soc London 134:235–253

Hekinian R, Moore JG, Bryan WB (1976) Volcanic rocks and processes of the Mid-Atlantic Ridge rift valley near 36°49′N. Contrib Mineral Petrol 58:83–110

Imsland P (1980) The petrology of the volcanic island Jan Mayen Arctic Ocean. Nordic Volc Inst Iceland, Int Rep 8003:1–501

Irvine TN (1977a) Definition of primitive liquid compositions for basic magmas. Carnegie Inst Wash Yearb 76:454–461

Irvine TN (1977b) Relative variations of substituting chemical components in petrologic fractionation processes. Carnegie Inst Wash Yearb 76:539–541

Irving AJ (1978) A review of experimental studies of crystal/liquid trace element partitioning. Geochim Cosmochim Acta 42:743–770

Johnson L, Monahan D (1979) Geomorphology of the Arctic Basin and adjacent continental margins. EOS 60:372

Kurz MD, Jenkins WJ, Schilling JG, Hart SR (1982) Helium isotopic variations in the mantle beneath the central North Atlantic Ocean. Earth Planet Sci Lett 36:133–156

LeMaitre RW (1962) Petrology of volcanic rocks. Gough Island, South Atlantic. Geol Soc Am Bull 73:1309–1340

Lussiaa-Berdon-Polve M, Vidal P (1973) Initial strontium isotopic compositions of volcanic rocks from Jan Mayen and Spitsbergen. Earth Planet Sci Lett 18:333–338

Maaloe S, Aoki K-i (1977) The major element composition of the upper mantle estmated from the composition of lherzolites. Contrib Mineral Petrol 63:161–173

Malod J, Mascle J (1975) Structures geologiques de la Marge Continentale a l'Ouest du Spitsberg. Marine Geophys Res 2:215–229

McMaster RL, Schilling JG, Pinet PR (1977) Plate boundary within Tjornes fracture zone on northern Iceland's insular margin. Nature 269:663–668

Melson WG, Vallier TL, Wright TL, Byerly G, Nelen J (1976) Chemical diversity of abyssal volcanic glass erupted along Pacific, Atlantic, and Indian Ocean sea-floor spreading centers. In: The Geophysics of the Pacific Ocean Basin and Its Margin. Am Geophys Union, Washington DC, pp 351–367

Mysen BO, Boettcher AL (1975a) Melting of a hydrous mantle: I. Phase relations of natural peridotite at high pressures and temperatures with controlled activities of water, carbon dioxide, and hydrogen. J Petrol 16:520–546

Mysen BO, Boettcher AL (1975b) Melting of a hydrous mantle: II. Geochemistry of crystals and liquids formed by anatexis of mantle peridotite at high pressures and high temperatures as a function of controlled activities of water, hydrogen, and carbon dioxide. J Petrol 16:549–599

Mysen BO, Kushiro I (1977) Compositional variation of coexisting phases with degree of melting of peridotite in the upper mantle. Am Mineral 62:843–865

Nielsen TFD (1978) The Tertiary dike swarms of the Kangerdlugssuaq area, East Greenland. Contrib Mineral Petrol 67:63–78

O'Nions RK, Pankhurst RJ (1974) Petrogenetic significance of isotope and trace element variations in volcanic rocks from the Mid-Atlantic. J Petrol 15:603–634

Pearce JA (1976) Statistical analysis of major element patterns in basalts. J Petrol 17:15–43

Pedersen S, Larsen O, Hall N, Campsie J, Bailey JC (1976) Strontium isotope and lithophile element values from the submarine Jan Mayen province. Bull Geol Soc Demn 25:15–20

Perry RK, Fleming HS, Cherkis NZ, Feden RH, Vogt PR (1980) Bathymetry of the Norwegian-Greenland and western Barents seas. Naval Res Lab Washington DC

Presnall DC, Dixon SA, Dixon JR, O'Donnell TH, Brenner NL, Schrock RL, Dycus DW (1978) Liquidus phase relations on the join diopside-forsterite-anorthite from 1 atm to 20 kbar: their bearing on the generation and crystallization of basaltic magma. Contrib Mineral Petrol 66:203–220

Presnall DC, Dixon JR, O'Donnell TH, Dixon SA (1979) Generation of mid-ocean ridge tholeiites. J Petrol 20:3–35

Schilling J-G (1973) Iceland mantle plume: geochemical study of Reykjanes Ridge. Nature 242:565–571

Schilling JG (1976) Petrochemical variations along the Mid-Atlantic Ridge from 29°N to 73°N. Trans Am Geophys Union 57:408

Schilling JG, Anderson RN, Vogt P (1976) Rare earth, Fe and Ti variations along the Galapagos spreading centre, and their relations along the Galapagos mantle plume. Nature 26:108–113

Schilling JG, Sigurdsson H (1979) Thermal minima along the axis of the Mid-Atlantic Ridge. Nature 282:370–375

Schilling JG, Zajac M, Evans R, Johnston T, White W, Devine JD, Kingsley R (1983) Petrologic and geochemical variations along the Mid-Atlantic Ridge from 29°N to 73°N. Am J Sci (in press)

Schmitt RA, Smith RH, Olehy DA (1964) Rare-earth, yttrium and scandium abundances in meteoritic and terrestrial matter – II. Geochim Cosmochim Acta 28:67–86

Shaw DM (1970) Trace element fractionation during anatexis. Geochim Cosmochim Acta 34:237–243

Sigurdsson H (1981) First-order major element variations in basalt glasses from the Mid-Atlantic Ridge: 29°N to 73°N. J Geophys Res 86:9483–9502

Sigurdsson H, Brown GM (1970) An unusual enstatite-forsterite basalt from Kolbeinsey Island, north of Iceland. J Petrol 11:205–220

Sigurdsson H, Schilling JG (1976) Spinels in Mid-Atlantic Ridge basalts, chemistry and occurrence. Earth Planet Sci Lett 29:7–20

Sparks RSJ, Meyer P, Sigurdsson H (1980) Density variations amongst mid-ocean ridge basalts: implications for magma mixing and the scarcity of primitive lavas. Earth Planet Sci Lett 46:419–430

Stosch HG (1982) Rare earth element partitioning between minerals from anhydrous spinel peridotite xenoliths. Geochim Cosmochim Acta 46:793–811

Stolper E, Walker D (1980) Melt density and the average composition of basalt. Contrib Mineral Petrol 74:1–12

Talwani M, Eldholm O (1977) Evolution of the Norwegian-Greenland Sea. Geol Soc Am Bull 88:969–999

Vogt PR, Perry RK, Feden RH, Fleming HS, Cherkis NZ (1981) The Greenland-Norwegian Sea and Iceland environment: Geology and geophysics, In: The Ocean Basins and Margins, vol. 5, Eds. Nairn AEM, Churkin M Jr, and Stheli IG, Plenum Publishing Co:493–598

Wagonner DG, Vollmer R, Schilling JG (1981) Isotopic and trace element variations along the Mohns and Knipovich Ridges. Trans Am Geophys Union 62:423

Walker D, DeLong SE (1981) Soret separation of mid-ocean ridge basalt magma. Contrib mineral Petrol 79:231–240

Walker D, Shibata T, DeLong SE (1979) Abyssal tholeiites from the Oceanographer Fracture Zone. Contrib Mineral Petrol 70:111–125

Weigand PW (1972) Bulk-rock and mineral chemistry of recent Jan Mayen basalts. Norsk Polarinst Årbok 1970:42–52

Weigand PW, Brunfelt AO, Heier KS, Sundvoll B, Steinnes E (1972) Geochemistry of alkali olivine basalts from an eruption on Jan Mayen. Nature Phys Sci 235:31–33

White WM, Schilling JG (1978) The nature and origin of geochemical variations in Mid-Atlantic Ridge basalts from the central North Atlantic. Geochim Cosmochim Acta 42:1501–1516

Wood DA, Tarney J, Varet J, Saunders AD, Bougault H, Joron JL, Treuil M, Cann JR (1979) Geochemistry of basalts drilled in the North Atlantic by IPOD leg 49: implications for mantle heterogeneity. Earth Planet Sci Lett 42:77–97

Received April 22, 1983; Accepted November 18, 1983